To Appear in The Astronomical Journal, July 1999
Preprint typeset using LaTeX style emulateapj

A 180 KPC TIDAL TAIL IN THE LUMINOUS INFRARED MERGER ARP 299

J.E. Hibbard
National Radio Astronomy Observatory[a], 520 Edgemont Road, Charlottesville, VA, 22903;
jhibbard@nrao.edu

[a]The National Radio Astronomy Observatory is a facility of the National Science Foundation operated under cooperative agreement by Associated Universities, Inc.

M.S. Yun
National Radio Astronomy Observatory[1], P.O. Box 0, Socorro, New Mexico, 87801; myun@nrao.edu

To Appear in The Astronomical Journal, July 1999

ABSTRACT

We present VLA H I observations and UH88″ deep optical B- and R-band observations of the IR luminous merger Arp 299 (= NGC 3690 + IC 694). These data reveal a gas-rich ($M_{HI} = 3.3 \times 10^9 M_\odot$) optically faint ($\mu_B \gtrsim 27$ mag arcsec^{-2}, $\mu_R \gtrsim 26$ mag arcsec^{-2}) tidal tail with a length of over 180 kpc. The size of this tidal feature necessitates an old interaction age for the merger ($\gtrsim$750 Myr since first periapse), which is currently experiencing a very young star burst ($\lesssim$20 Myr). The observations reveal a most remarkable structure within the tidal tail: it appears to be composed of two parallel filaments separated by ∼20 kpc. One of the filaments is gas rich with little if any starlight, while the other is gas poor. We believe that this bifurcation results from a warped disk in one of the progenitors. The quantities and kinematics of the tidal H I suggest that Arp 299 results from the collision of a retrograde Sab-Sb galaxy (IC 694) and a prograde Sbc-Sc galaxy (NGC 3690) that occurred 750 Myr ago and which will merge into a single object in ∼ 60 Myr. We suggest that the present IR luminous phase in this system is due in part to the retrograde spin of IC 694. Finally, we discuss the apparent lack of tidal dwarf galaxies within the tail.

Subject headings: galaxies: evolution — galaxies: individual (NGC 3690, IC 694, Arp 299) — galaxies: interactions — galaxies: ISM — galaxies: kinematics and dynamics — galaxies: peculiar — galaxies: starburst — infrared: galaxies

1. INTRODUCTION

Arp 299 is a nearby (V_{hel}=3080 km s^{-1})[1] peculiar system comprised of two highly distorted disk galaxies, with NGC 3690 (= Mrk 171A = UGC 6471 = VV118b) to the west and IC 694 (= Mrk 171B = UGC 6472 = VV118a)[2] to the east. There is also a compact spheroidal galaxy lying approximately 1′ to the NW which is a the same velocity as Arp 299 (MCG+10-17-2a, V_{hel}=3100 km s^{-1}, Fairall 1971, Sargent 1972). Figure 1 presents a B-band image of this system, taken from the optical data described later in this paper. Each of the above named systems are labeled, as is the unrelated background bridge-tail-bar system Arp 296.

Arp 299 appears to be in an advanced stage of merging, with the two disks in contact, but the nuclei still separated by about 20″ (4.7 kpc)[3]. This impression is supported by radio continuum and near-infrared (NIR) imaging (Gehrz, Sramek & Weedman 1983) and millimeter spectral line observations (Casoli *et al.* 1989, 1999; Sargent & Scoville 1991, Aalto *et al.* 1997), which locate two major concentrations of molecular gas at peaks in the radio and NIR (regions **A** and **B** in Fig. 1, using the naming convention of Gehrz, Sramek & Weedman 1983). Source **A** is identified with the nucleus of IC 694, while source **B** is identified with the nucleus of NGC 3690.[4] Another concentration of molecular gas occurs at the region of disk overlap (labeled **C-C′** in Fig. 1).

Spectroscopic observations of the NIR peaks in radio recombination lines (Anantharamaiah *et al.* 1993; Zhao *et al.* 1997), the Mid infrared (Dudley & Wynn-Williams 1993; Dudley 1998), the NIR (Gehrz, Sramek & Weedman 1983; Beck, Turner & Ho 1986; Nakagawa *et al.* 1989; Ridgeway, Wynn-Williams & Becklin 1994; Doherty *et al.* 1995; Smith *et al.* 1996; Lançon, Rocca-Volmerang & Thuan 1996), optical recombination lines (Bushouse & Gallagher 1984; Keel *et al.* 1985; Armus, Heckman & Miley 1989) and in the UV (Augarde & Lequeux 1985; Kinney *et al.* 1993; Roberts 1996; Vacca *et al.* in preparation) fail to reveal any definitive evidence for an AGN, and are consistent with the dominant energy source being a compact starburst (although there is evidence for some contribution due to a compact source; see Shier, Rieke & Rieke 1996; Carral, Turner & Ho 1990; Jones *et al.* 1990; Jones 1997). This picture is consistent with continuum observations in the radio (Condon *et al.* 1982; Gehrz, Sramek &

[1]All radial velocities quoted in this paper are heliocentric.

[2]There is some confusion as to the naming of this system, which is addressed separately in the appendix. In the following, we following the naming convention used most widely in the literature.

[3]Adopting the distance of 48 Mpc from Sanders, Scoville & Soifer (1991), which assumes H_o=75 km s^{-1} Mpc^{-1} and the Virgocentric flow model of Aaronson *et al.* (1982). At this distance 1′=14 kpc.

[4]High resolution NIR imaging by Wynn-Williams *et al.* (1991) shows that source **B** is itself a double, separated by about 3″.

Weedman 1983; Condon *et al.* 1990, 1991; Smith, Lonsdale & Lonsdale 1998), far infrared (Joy *et al.* 1989), NIR (Telesco, Decher & Gatley 1985; Carico *et al.* 1990; Wynn-Willams *et al.* 1991; Miles *et al.* 1996), and X-ray (Rieke 1988, Zezas *et al.* 1998).

Within the main body, vigorous star formation is taking place, with an inferred star formation rate (SFR) of $\sim$50 $M_\odot\,\mathrm{yr}^{-1}$ (Heckman, Armus & Miley 1990), and an age of $\lesssim$20 Myr (Augarde & Lequeux 1985; Stanford 1989; Nakagawa *et al.* 1989; Meurer *et al.* 1995; Vacca *et al.* in preparation). A deep Hα + [N II] image of this system reveals a "magnificent large-scale filamentary structure made up of arcs and loops that surround the galaxies at radii $\sim$ 6–12 kpc" (Armus, Heckman & Miley 1990). Recent x-ray observations reported by Heckman *et al.* (1999) show evidence for hot gas emerging from the inner regions to the north, which the authors interpret as evidence for a hot, expanding superwind fluid.

The present Very Large Array (VLA) 21cm observations of the neutral hydrogen (H I) in Arp 299 were conducted as part of a larger program to study the closest luminous IR galaxies in the IRAS Bright Galaxy Sample of Sanders *et al.* (1991). Arp 299 is both the most IR luminous member of this sample within a distance of 50 Mpc ($L_{IR} = 8.1 \times 10^{11} L_\odot$), and the closest system with an IR luminosity greater than $5{\times}10^{11} L_\odot$. It is therefore an important target to study for insight into the causes of such luminous starbursts. The purpose of the present study is to map any extended atomic hydrogen in order to constrain the encounter geometry and the Hubble types of the progenitors.

The paper is organized in the following manner. In §2 we briefly describe the observations. In §3 we present the observations separately for the inner regions, tidal regions, and for the H I absorption and a new H I detected companion. In §4 we use the observations to explore the probable Hubble types of the progenitors, the encounter geometry, the possibility of self-gravitating entities within the tail, the conditions for an IR luminous phase, and the explanation for the differing H I and optical tidal morphologies. We summarize our main conclusions in §5.

2. OBSERVATIONS

2.1. *HI Observations*

The VLA H I spectral line observations were obtained as part of a study on the outer gas dynamics of IR luminous mergers (Hibbard & Yun 1996 and in preparation), and the data reduction techniques are fully described in that paper, except for the continuum subtraction which is described below. The details of these observations are tabulated in Table 1. Briefly, the data consist of a 3.5 hour observation with the VLA in the C-array configuration (full-width at half maximum resolution $\theta_{FWHM}{\sim}15''$) and a 3 hour observation with the VLA in the D-array configuration ($\theta_{FWHM}{\sim}45''$). The data were combined in the UV plane to form the C+D array data that are used in the remainder of this paper. The correlator mode was chosen to provide 63 spectral channels with a channel spacing of 10.5 km s^{-1} and total bandwidth of 660 km s^{-1} centered at 3080 km s^{-1}. The data were reduced using standard reduction procedures in the Astronomical Image Processing System (AIPS).

The observations reveal broad H I absorption against the disk-wide starburst and central radio continuum sources (see also Dickey 1982; Baan & Haschick 1990 hereafter BH90). This absorption was observed in channels 5–55 out of the 63 channel data cube (of which only channels 2–58 are useful). As a result, we could not achieve an optimal continuum subtraction by using line free channels on either end of the bandpass, as is usually done (e.g. Rupen 1999). Instead, we mapped and "cleaned" the continuum image and subtracted the brightest 17 "clean components" from the UV line data, which accounts for approximately half of the total continuum flux of 820 mJy falling within the primary beam (FWHM=30$'$). The line data were then mapped and cleaned in AIPS, resulting in a three dimensional H I data "cube", with Right Ascension and Declination along the first two coordinates and velocity along the third axis.

These data still contained many continuum sources, but were relatively free of the deep sidelobes from the brighter sources. The residual continuum was removed in the map plane using a spatially variable continuum baseline. The H I tidal features appeared over a narrow range of velocity, and the residual continuum was removed from these regions by fitting a first order polynomial to a large number of channels on either side of this range. The emission from the NW disk appears in channels 4–26, and the residual continuum was subtracted from this region by fitting to the continuum in channels 34–54. The emission from the SW disk appears in channels 24–50, and the residual continuum was subtracted from this region by fitting to the continuum in channels 4–20. Finally, the residual continuum was removed from the regions showing H I absorption by fitting to the continuum in channels 2–4 and 52–58.

The data were mapped using different weighting functions to achieve varying resolutions and sensitivities. A high resolution data cube was made using a "Robust" parameter (R; Briggs 1995) of R=0, which gives more weight to longer baselines and hence to smaller angular scales. This cube obtains a surface brightness sensitivity of 0.35 mJy beam^{-1} at a resolution of θ_{FWHM}=17$''{\times}$15$''$. This corresponds to a column density limit (2.5σ) of $4{\times}10^{19}$cm^{-2} averaged over the beam width of 4.0×3.4 kpc^2. A more sensitive intermediate resolution data cube was made with R = 1, giving a resolution of 22$''{\times}$20$''$ (5.1×4.7 kpc^2) and a column density limit of $2{\times}10^{19}$cm^{-2}. To further increase sensitivity to extended low column density gas, a low resolution data cube was made by convolving the R=1 data cube to a resolution of 35$''$ (8.1 kpc), reaching a detection limit of $1{\times}10^{19}$cm^{-2}. These data will be referred to in the following as the high, intermediate, and low resolution data, respectively.

2.2. *Optical Observations*

The VLA observations reveal a gaseous stream of material extending to a radius of 9$'$ that had no known optical counterpart on existing images. As such, this region was targeted for deeper optical observations with the University of Hawai'i 88$''$ telescope at Mauna Kea Observatory. The observational parameters are listed in Table 2. The Tek 2048 CCD was used with the f/10 re-imaging optics, giving a plate scale of 0.22$''$ pixel^{-1} and a field of view of 7$'\!.$5. Three overlapping 600 sec R-band images of the region of interest were obtained in January 1995. In January 1997 we obtained a 600 sec B-band image centered on the main body and two overlapping 900 sec B-band images of the H I tail. The total imaged region covers an area of $8'.7\times12'.4$. The conditions were photometric on both dates, and the seeing was $\sim1''$. The data were calibrated via observations of Landolt UBVRI standards (Landolt 1983) observed on the same nights, with zero point errors (1σ) of 0.01^m in B and 0.03^m in R.

The images were flattened and combined using the techniques described in Hibbard & van Gorkom (1996, hereafter HvG96), and the final mosaics are flat to better than one part in 500. The combined image was transformed to the World Coordinate System (and thereby to the same reference frame as the radio images) by registering to an image of the same area extracted from Version II of the Digitized Sky Survey[5] (XDSS), obtained from the CD jukebox at the Canadian Astronomy Data Centre.[6] The registration was accomplished by referencing the location of ~20 stars in common on both images using the "koords" program in the Karma software package (Gooch 1995) to perform a non-linear least squares fit for the transformation equations. The plate solution so found is better than a fraction of a pixel ($0.22''$), and the overall registration should be as good as that of the northern portion of the Guide Star Catalog, which is estimated to be $0''.5$ (Taff *et al.* 1990).

Finally, a deep optical image was constructed by binning the pixels with the lowest light levels 9x9 to achieve a limiting surface brightness of μ_B=28.2 mag arcsec^{-2} and μ_R=27.1 mag arcsec^{-2} (2.5σ; Table 2).

3. RESULTS

The luminosity for the main galaxies was calculated out to the μ_B=26 mag arcsec^{-2} isophote, and the corresponding B magnitude for the Arp 299 system (m_B=12.31) agrees within 0.01^m to that given by Mazzarella & Boroson (1993). These and other global parameters for the Arp 299 system are given in Table 3, and the entries are described in the notes to that table. In the following, we will discuss the kinematics and morphology of the inner disk first, and then that of the outer tidal features. We also discuss the central H I absorption and report the discovery of a small dwarf companion to Arp 299.

3.1. *Inner Gas Disk*

The disk H I kinematics are illustrated in Figures 2 & 3. Fig. 2 presents several 2-dimensional representations of the high resolution H I data, with the emission summed over the third dimension. The upper left panel shows the integrated intensity map in solid contours (lowest contour corresponds to $N_{HI}\sim5\times10^{19}$cm^{-2}) upon the B-band image. This map emphasizes higher column density material at the expense of the diffuse lower column density H I. We have therefore provided a dotted contour to indicate the $N_{HI}=2\times10^{19}$cm^{-2} contour of the intermediate resolution data, in order to give a more complete picture of the H I distribution in the inner regions. We have also labeled a minor axis clump of H I and a western plume for reference in the following discussion.

To the right and below this panel are position–velocity maps constructed by summing the emission over declination (lower panel) or right ascension (right panel). Fig. 3 presents the high resolution channel maps of the inner disk alone, after Hanning smoothing by a factor of two in velocity. In both of these maps, absorption is indicated by white dashed contours.

The inner H I disk was previously mapped with the VLA in the C-array configuration by Stanford & Wood (1989). As discussed by these authors, the kinematic signature seen in Figs. 2 & 3 is representative of a rotating disk, with the NW half of the disk receding and the SW half approaching. The NW component of the disk reaches a radius of 25 kpc and contains $2.9\times10^9M_\odot$ of H I. The SE component of the H I disk reaches a radius of 21 kpc and contains a total of $2.8\times10^9M_\odot$ of atomic hydrogen.[7] The disk spans the velocity range from 2880–3390 km s^{-1}, with its kinematic center at 3135 km s^{-1}.

This disk was also mapped by the VLA in the D-configuration by Nordgren *et al.* (1997) using a coarser velocity resolution (by a factor of four) and a larger bandpass (by a factor of two) than the observations presented here. Their observations suggest that the emission from the NW disk continues to 3550 km s^{-1} (see their Fig. 7b), and therefore it is likely that we have missed some disk emission due to our smaller velocity coverage. The OH maser emission from Arp 299 (Baan 1985; BH90) suggests that there may be nuclear gas at velocities as high as 3650 km s^{-1}.

The H I disk appears to be physically associated with the optically distorted disk of IC 694. This view is strongly supported by both the CO and Hα kinematics mapped at higher spatial resolution, as will be discussed in §4.1 below. There are, however, emission features which deviate from this simple disk motion. There are $4.6\times10^8M_\odot$ of gas in a western extension to the NW portion of the disk, and which appears kinematically associated with that disk (*i.e.*, appears in the same velocity channels in Fig. 3), but which is spatially associated with a faint plume of starlight reaching to the SW (labeled "western plume" in Fig. 2, see also Fig. 1). There are also $1.5\times10^8M_\odot$ of gas in a clump lying along the SW minor axis of the disk (labeled "minor axis clump" in Fig. 2). If this minor-axis material were associated with the disk of IC 694, it should appear in only a few spectral channels. Since it appears over a broad range of velocities (from 3050—3200 km s^{-1} in Fig. 3), we suggest instead that it is associated with NGC 3690 (see §4.1). There is also some emission associated with the base of the tidal tail (seen in the right panel of Fig. 2 towards the north and in the channel maps from 3092—3135km s^{-1}), which is seen more clearly in the low resolution maps discussed in the next section. Finally, there are some H I features that project close to the compact spheroidal galaxy MCG+10-17-2a (Fig. 3, channels at 3306—3371 km s^{-1}). Since these

[5] The Second Palomar Observatory Sky Survey was made by the California Institute of Technology with funds from the National Science Foundation, the National Geographic Society, the Sloan Foundation, the Samuel Oschin Foundation, and the Eastman Kodak Corporation. The Oschin Schmidt Telescope is operated by the California Institute of Technology and Palomar Observatory.

[6] The Canadian Astronomy Data Center is operated by the Dominion Astrophysical Observatory for the National Research Council of Canada's Herzberg Institute of Astrophysics.

[7] These masses do not include the contributions due to gas in the western plume or minor axis clump discussed later.

features appear at velocities that are higher than the velocity of MCG+10-17-2a itself (V_{hel}=3100 km s^{-1}, Fairall 1971, Sargent 1972), and close to the velocites of the H I within the underlying disk of IC 694, it seems likely that they are due to disk material that was perturbed by a recent close passage of the spheroidal.

3.2. *Outer Tidal Morphology*

Our VLA observations revealed a previously unknown tidal tail reaching 124 kpc in radius to the north. This discovery was initially reported in Hibbard & Yun (1996). Subsequently, VLA D-array observations of Arp 299 from May 1995 were published by Nordgren *et al.* (1997), confirming both the H I and optical tidal tail we report on in this paper.

In Figure 4 we show the H I integrated intensity map from the intermediate resolution data, with position-velocity profiles plotted along either axis as in Fig. 2. The tail appears as two parallel filaments separated by about 20 kpc (labeled "inner filament" and "outer filament" in Fig. 4), extending northward and connecting onto or merging into a dense clump of gas (labeled "N clump" in Fig. 4). The inner filament originates near the minor axis of IC 694 (see also the northernmost clump in Fig. 2), appears broken at the lowest contour drawn in Fig. 4 (N_{HI}~2.5×10^{19}cm^{-2}) after which there appears an H I density peak ($N_{HI,peak}$ ~ 2×10^{20}cm^{-2}, labeled "H I knot" in Fig. 4), and the filament continues northward. This inner filament contains a total of 4.4×10$^8 M_\odot$ of neutral atomic hydrogen. The outer filament originates to the west of the first (see also the second northernmost clump in Fig. 2), is more complete and of a higher average column density than the inner filament (N_{HI}~1×10^{20}cm^{-2}), and contains twice as much H I (M_{HI}=9×10$^8 M_\odot$). The filaments join at the N clump, which contains 2×10$^9 M_\odot$ of H I. This clump has an irregular column density distribution with peaks as high as 3×10^{20}cm^{-2}. The kinematics of these features will be discussed in the next section.

The tail reaches a maximum projected radial separation of 8$'$.6 (124 kpc; measured from source **A** to the outer contour in Fig. 4), and extends 12$'$.7 or 180 kpc as measured along its length (measured from source **A** along the peak H I column density contour of the outermost feature). It contains a total of 3.3×10$^9 M_\odot$ of atomic hydrogen, which is at the upper end of the tidal gas content of other major disk-disk mergers (HvG96, Hibbard & Yun in preparation). Since less than half of the progenitor disk material can be raised into a tail, and most of this falls back quickly onto the remnant (Hibbard & Mihos 1995), this amount of tidal H I requires a very H I rich progenitor (M_{HI} ~ 10$^{10} M_\odot$). This point will be explored in more detail in §4.2.

The deep optical imaging reveals a faint stellar tail extending in the same direction as the H I features (see Figures 5, 6 & 7). The optical tail appears to emerge in the north near the minor axis of the system and curve slightly to the NE to a radius of 9$'$. The width of the optical tail appears remarkably constant at ~1$'$ (14 kpc), although there may be some widening in the B-band image. The observed width of the tail can be understood as the result of the dispersal of outer disk stars with a typical velocity dispersion of 20 km s^{-1}(e.g. van der Kruit 1988; Bottema 1993) over an interaction age of 750 Myr (§4.1). At very faint light levels the tail appears to loop south and west from the NE tip towards the bright star labelled "Star 2" in Fig. 5a, with perhaps a very faint extension directly south of this star. While scattered light from the stars labelled 1 & 2 in this figure make the precise morphology of the faint optical light uncertain, these features have the same morphology in both the B- and R-band greyscale images of Fig. 5, while the scattered light properties are different between the bands (see e.g. the difference between the faint scattered light associated with Star 3 in Figs. 5a & 5b), and we feel confident that the faint optical features are not artifacts.

Upon first examination the optical and H I tidal features appear similar. But when the data are overlaid, as in Figs. 6 & 7b, the differences in the distribution are striking: the inner H I filament roughly aligns with the optical tail, while the outer parallel H I filament has no corresponding optical feature down to the faintest levels measured (μ_B~28.5 mag arcsec^{-2}, μ_R~27.5 mag arcsec^{-2}).

Even within the optical tail, there is a poor correlation between optical and gaseous density peaks. If anything, the gas peaks seem to be displaced a bit to the west of the optical peaks. Neither the gap nor the knot in the inner H I filament appear to coincide with any discrete optical feature, although the optical surface brightness drops by ~1 mag arcsec^{-2} just north of the knot (Fig. 5). The displacements are even more extreme in the northernmost regions of the tail, where the gas and starlight appear to be anti-correlated: to either side of the optical tail there are regions of high gas column density (N_{HI}~3×10^{20}cm^{-2} to the west, N_{HI}~2×10^{20}cm^{-2} to the east), whereas the gas within the tail has N_{HI}~1×10^{20}cm^{-2}. At its northernmost extent, the optical tail has no associated H I, and actually appears to "hook" towards the east, *exactly* around the northern H I contours in Fig. 7b.

This anti-correlation suggests the possibility that dust associated with the H I gas is playing a role in shaping the optical tidal morphology. It is possible that extinction affects te optical morphology at the lowest light levels (e.g. at the northernmost "hook", $\mu_B \gtrsim$28mag arcsec^{-2}). However, it is not likely to be hiding an optical counterpart to the outer filament since the required amount of extinction (>1 mag at N_{HI}= 2×10^{20}cm^{-2}) is an order of magnitude larger than measured for Galactic H I (Bohlin *et al.* 1978). Since tails are drawn from the outer, presumably dust-poor regions of disks, such a high gas-to-dust ratio seems unlikely (see also Alton *et al.* 1998). Evidence for just such a high gas-to-dust content in tidal gas may be indicated by observations of red globular clusters behind an HI tidal stream in NGC 5018 (Hilker & Kissler-Patig, 1996). Still, we feel that this explanation is ruled out for Arp 299 by the fact that the optical tail is actually bluer north of the H I knot, where the H I column density is highest, compared to the starlight in the "gap" in the inner H I filament, where the H I column density is lowest (Fig. 7a). One would expect the opposite trend if there was a high gas-to-dust ratio in this tidal gas (however see Witt, Thronson & Capuano 1992). The $B-R$ colors of the stellar tail range from 0.3–1.8, similar to range found in the outer stellar disk of late type galaxies (de Jong 1995, Ch. 4) and in other tailed mergers (Schombert *et al.* 1990; Hibbard *et al.* 1994; Hibbard 1995).

The total stellar content of the optical tail was estimated by masking the optical images below μ_B= 28 mag arcsec^{-2}and μ_R= 27 mag arcsec^{-2} and replacing regions containing point sources (presumably background sources, §4.5) and the optical halos of Stars 1& 2 in Fig. 5a with adjacent background values. The total optical light in the northern tail is $L_B = 1.6 \times 10^9 L_{\odot,B}$ and $L_R = 1.2 \times 10^9 L_{\odot,R}$, corresponding to 4% and 2% of the total B- and R-band light of the system, respectively[8] (Table 3). These percentages are on the lower end of the values found in peculiar systems (Schombert *et al.* 1990; Hibbard *et al.* 1994; HvG96).

The total H I mass-to-blue light ratios (in solar units) for all the northern tidal features is M_{HI}/L_B= 1.8. There is quite a variation within the tail, with M_{HI}/L_B ~0–1 along the optical tail, and ranging from 2 to over 10 for the outer filament and eastern regions of the N clump. The faint plume of light extending 45 kpc in radius to the west of Arp 299 contains $L_B = 1 \times 10^9 L_{\odot,B}$. Associating the western H I extension to this feature gives M_{HI}/L_B=0.5.

3.3. *Outer Tidal Kinematics*

The kinematics of the tidal regions are illustrated by the integrated position-velocity profiles in Fig. 4, intensity weighted velocities and velocity dispersions in Fig. 7c&d, individual channel maps in Fig. 8, and two position-velocity slices through either H I filament in Fig. 9. Both Fig. 8 and Fig. 9 are constructed from the low resolution data cube, and the lowest plotted contour corresponds to a column density of $1{\times}10^{19}$cm^{-2}. The channel maps are only plotted over the velocity range containing tail emission.

The kinematics immediately illustrate two important points. The first is that the tidal kinematics are smooth, continuous and single valued, as expected for tidal features (e.g. Barnes 1988; Hibbard *et al.* 1994; Hibbard & Mihos 1995). The second is that the two H I filaments s hare the same kinematics. This is best seen in Fig. 8, in which the H I emission associated with parallel regions along the filaments appears in identical channels all along the tail. This rules out the possibility that the two filaments are separate tidal tails that are simply projected near each other; they must be different regions of the same kinematic structure. The figures also show that the N clump is continuous with the filaments and not a distinct entity. Therefore, the N clump and two filaments form a single contiguous feature in both space and velocity.

A more detailed comparison of the filament kinematics is shown in Fig. 9, where we have plotted position-velocity profiles along both. This figure shows that the base of the outer filament has a slightly higher mean velocity than the base of the inner filament, which may help in deciding the relative morphologies, although we await detailed kinematic modeling before deciding how to interpret this information. Fig. 9 illustrates a few more interesting properties of the filaments. In Fig. 9b we see that the apparent "gap" in the integrated intensity map of Fig. 4 is not devoid of H I: weak emission which did not pass the threshold used when making the moment maps bridges this gap (see also the panel at 3150 km s^{-1} in Fig. 8). We also see that the "knot" within the inner filament has an anomalously large velocity width (see also line-width map in Fig. 7d): the majority of the tail has a velocity dispersion of 7–9 km s^{-1}, which is typical of tidal tails in general (Hibbard *et al.* 1994, HvG96), while the knot has a dispersion of over twice this (20 km s^{-1}). Fig. 7d shows that there are two additional velocity dispersion peaks along the southern edge of the N clump, with dispersions of 17 km s^{-1} and 13.5 km s^{-1} compared to an average dispersion of 10.5 km s^{-1} within the N clump. None of these regions corresponds to any noticeable features in the optical images or color maps, which argues against their being related to the putative tidal dwarf galaxies, a question we investigate in more detail in §4.5.

Finally, there is a high velocity envelope of material just north of the knot (indicated in Fig. 9b). A similar envelope of material is seen at parallel locations in the outer filament (Fig. 9d). The channel maps show that this gas lies exactly along the faint optical light that stretches from the end of the tail towards Star 2 in Fig. 5a (see panels at 3171–3161 km s^{-1} in Fig. 8), while the majority of the filament gas has lower velocities and lies north of this light (see panels at 3098–3140 km s^{-1} in Fig. 8). These are probably important clues to the origin of these filaments, although we are at a loss to say what.

3.4. *Central Absorption*

High resolution (~5″) VLA radio continuum observations show that half of the 1.4 GHz radio continuum emission lies within 5″ of regions **A, B** and **C-C′** in Fig. 1, with the other half of the flux distributed between these regions and throughout the disk of IC 694 (Gehrz, Sramek & Weedman 1983). Even higher resolution (θ_{FWHM}=1.″7) VLA A-array observations of the H I absorption against these continuum sources are presented in BH90, along with observations of OH megamaser emission. These observations show that H I absorption is seen against all of the compact continuum sources as well as against the extended continuum features. Our continuum profiles are quite similar to those published by BH90, with subtle differences that are likely due to our larger beam, which allows surrounding H I emission to fill in some of the absorption. We will therefore use the results of the higher resolution H I absorption observations in concert with our H I emission observations to set some rough limits on the spin temperature (T$_{\rm spin}$) of the H I gas. Along the way, we will estimate the absorbing column of gas in front of the continuum sources, from which we will derive an approximate correction to the total H I mass.

BH90 found that the H I absorption is dominated by a broad component (ΔV ~120 km s^{-1}) at V_{hel}=3160 km s^{-1}, and a narrow component (ΔV ~70 km s^{-1}) at V_{hel}=3050 km s^{-1}. Due to the near correspondence of these velocities with the systemic velocities of IC 694 and NGC 3690 (3080–3180 km s^{-1}and 3000–3080 km s^{-1}, respectively; BH90 and reference therein) and because these two components are found in the absorption spectrum against *all* of the radio continuum sources, BH90 deduce that they are due to outer disk material from both IC 694 and NGC 3690 lying in the foreground rather than near-nuclear gas clouds. This allows us to interpolate our H I

[8]These numbers increase to $L_B = 2.1 \times 10^9 L_{\odot,B}$ (5%) and $L_R = 1.9 \times 10^9 L_{\odot,R}$ (4%) if the background point sources are left in and a 0.5 mag arcsec^{-2} lower surface brightness threshold is used.

column density maps across the absorbing regions. This column density can then be used together with the ratio of the neutral gas absorbing column density to the spin temperature ($N_{HI}/T_{\rm spin}$) given by BH90 to constrain T_{spin}.

From the column densities given in Fig. 2, we estimate a foreground column density of $N_{HI} \approx$1–2$\times10^{21}$cm^{-2} due to the disk of IC 694. For the corresponding absorption component (i.e. the broad component at V_{hel}=3050 km s^{-1}), BH90 find $N_{HI}/T_{\rm spin} \sim$3–8$\times10^{19}$cm^{-2} f_g K^{-1}, where f_g is the fraction of the radio continuum source covered by absorbing gas. Since BH90 find this absorption feature in the spectra of *each* continuum source in Arp 299, f_g must be near unity, yielding a spin temperature of 12–70 K. This is similar to the range found in our galaxy (34–74 K; Kalberla *et al.* 1985). The lower range of temperatures are similar to the very low values of T$_{\rm spin}$ (T$_{\rm spin}$ < 50 K) found in the Magellanic stream (Kobulnicky & Dickey 1999) and the nearby galaxies NGC 247 and NGC 253 (Dickey, Brinks & Puche 1992).

Using this range of spin temperatures and the measured $N_{HI}/T_{\rm spin}$ values from BH90 for the low velocity absorption component (V_{hel}=3050 km s^{-1}, $N_{HI}/T_{\rm spin}$ = 1–2$\times10^{19}$cm^{-2} K^{-1}) we deduce a column density of $10^{20}-10^{21}$cm^{-2} due to gas from NGC 3690. Adding these two contributions[9] gives an expected column density of 1–3$\times10^{21}$cm^{-2} in front of the absorption region. Doubling these values to account for emission behind the continuum sources we conservatively estimate an average column density in the absorbing region of 2×10^{21}cm^{-2}, corresponding to a "missing" H I mass of $2.2\times10^9 M_\odot$. This value is used to arrive at the "absorption corrected" M_{HI} value tabulated in Table 3. This total is very approximate, and could easily be 2–3 times as large (see §4.2).

3.5. *HI Detected Companion*

The H I observations uncovered a previously unknown and uncataloged companion to Arp 299 containing $8 \times 10^7 M_\odot$ of H I. This companion lies $\sim$10′ west and 3′ south of Arp 299 (projected separation of r=140 kpc) and has a systemic velocity of +145 km s^{-1} with respect to Arp 299. This region was not covered in our optical observations. An amorphous optical counterpart is found at this location on the XDSS image. The H I column density is contoured upon the XDSS image in Figure 10, and channel maps are shown in Figure 11.

We attempt to derive an optical luminosity for this companion from the POSS-E plate of Version I of the DSS, using the photometric solution given at *http://www-gsss.stsci.edu/dss/photometry/poss_e.html*. However, the number of counts from this source (log[counts] = 4.52) is lower than the levels over which calibration has been reliably determined (log[counts] = 4.8, m_{POSS-E} < 16 mag). Extrapolating the faint end of the above curve to the observed number of counts gives a somewhat uncertain estimated magnitude of m_{POSS-E}=17 mag. Assuming an average value of $B-R$ = +1.0 (e.g. van Zee, Haynes, & Salzer 1997), the absolute B magnitude of the H I companion is about $M_B = -15.4$.

The resulting global properties for the companion are given in Table 3. The optical appearance and H I properties of this system are similar to those of dwarf irregulars (Hoffman *et al.* 1996), and it is likely to have been a dwarf irregular companion of one of the progenitors. For comparison, it is about 20 times fainter and 30 times less gas-rich than the LMC (Tully 1988).

4. DISCUSSION

Although the differences between the optical and gaseous tidal morphology are bizarre, the tail kinematics and general morphology are very similar to the gas-rich tails of more classically understood mergers (e.g. Schweitzer 1978; van der Hulst 1979; Hibbard *et al.* 1994; HvG96), and the two main bodies certainly appear to be separate disk systems that have been strongly perturbed. It therefore seems that the tidal hypothesis — that these features arise as a result of two spiral galaxies falling together under their mutual gravitational attraction and merging due to the effects of dynamical friction (e.g. Toomre & Toomre 1972 hereafter TT72; Barnes & Hernquist 1996) — still provides the simplest explanation for the many peculiarities in this system.

Given this premise, we now aim to understand the gross characteristics of the encounter: what was the general encounter geometry (§4.1), and what were the approximate Hubble types of the progenitors (§4.2)? We explore possible explanations for the differences between the gaseous and stellar tidal features in §4.3, although much of this discussion is deferred to a separate paper (Hibbard, Vacca & Yun 1999, hereafter HVY99). In §4.4 we examine what, if anything, the state of this system tells us about the conditions under which super starbursts are initiated, leading to an ultraluminous infrared phase. Finally, in §4.5 we discuss the lack of putative tidal dwarf galaxies in the outer tidal features.

4.1. *The Nature of the Encounter*

The tail kinematics do not themselves determine the spin geometry of their progenitor. This is because the line-of-sight velocity fields of tidal features are often dominated by projection effects. This is particularly true of long filamentary tails, for which the space velocities will be oriented primarily perpendicular to our line-of-sight (leading directly to their large apparent lengths). Instead, we use the morphology of the tail to deduce the relative spin geometry between its progenitor disk and the orbital plane. In particular, only disks with a prograde spin geometry (*i.e.*, a spin angular momentum roughly aligned with the orbital angular momentum of the two merging galaxies) can raise such long, drawn out features (TT72, Barnes 1988), and the progenitor of the northern tail must have had just such a prograde spin orientation.

Further, since tidal tails remain close to the original spin plane of the disk from which they are extracted (TT72), and the observed tail in Arp 299 emerges at nearly right angles to the disk of IC 694, we conclude that IC 694 could not have generated this feature. The tail must therefore have arisen from NGC 3690. Similarly, the lack of any narrow drawn-out features near the plane of the disk of IC 694 suggest that this system experienced the encounter

[9] There are additional absorption components seen in the H I absorption spectra obtained by BH90, but their association with OH emission features at similar velocities places them very close to the nucleus of IC 694 with a small covering factor, and they will therefore contribute very little to the total H I mass.

in a highly inclined or retrograde sense. Such encounters provoke a much milder kinematic response in a disk (e.g. TT72; White 1979; Noguchi 1991), accounting for the survival of the disk morphology and kinematics of IC 694 so late into the encounter. This spin geometry agrees with the kinematics of the inner regions derived from Hα emission line kinematics, which show that IC 694 and NGC 3690 rotate in opposite directions (Augarde & Lequeux 1985; Hibbard, Bland-Hawthorn & Tully, in preparation). Further, the systemic velocities for the two nuclei ($V_{hel} \approx$ 3135 km s^{-1} for IC 694 [§3.1] and $V_{hel} \approx 3040$ km s^{-1} for NGC 3690 [§3.4]) give them the proper sense of motion for the inferred spin geometry — the nuclei rotate about each other opposite the direction that the disk of IC 694 rotates.

The morphology and kinematics of the ionized gas in Arp 299 has been mapped with a Fabry-Perot interferometer (Hibbard, Bland-Hawthorn & Tully, in preparation), showing that there is spatial and kinematic continuity between the outer H I disk all the way inward to source **A**. This implies that the entire disk structure belongs to IC 694; *i.e.* the H I is not distributed in a settled disk in rotation about both systems, as suggested by Stanford & Wood (1989). Further, these observations reveal that NGC 3690 and sources **B & C-C′** are kinematically distinct from the IC 694 disk, as expected from the inferred prograde-retrograde spin geometry.

From the redshifted velocities along most of the outer tail, and the fact that the tail should be predominantly in expansion along most of its length (Hibbard & Mihos 1995), we deduce that the tail curves away from us and should connect to the main bodies from behind. In this case, the decrease in velocities seen at the very base of the tail in Fig. 9b (third arrow from the bottom in both figures; see also northern region of upper right panel in Fig. 2), indicates that the material at the base of the tail has reached its apocenter and is falling back to smaller radii (e.g., Hibbard *et al.* 1994; Hibbard & Mihos 1995). Similarly, the broad range of velocities seen for the minor axis clump of H I (Fig. 3) suggests that this material is part of the northern tail connecting back to its progenitor, NGC 3690. If there is more H I associated with the disk of NGC 3690, it would be difficult to disentangle from the emission due to the SW portion of the disk of IC 694 and the central HI absorption.

Finally, the western plume may be disk material from IC 694 that was perturbed during an earlier pericentric passage of the two galaxies about each other or by the passage of the compact NW spheroidal (MCG+10-17-2a). Since tidal material tends to lie within the plane it occupies at the time it is raised (TT72), the distribution of this gas should reflect the plane of the disk of IC 694 at an earlier stage of the merger, perhaps at an early pericentric approach. The fact that this plane is different from the present plane suggests that the angular momentum of the disk was changed during the encounter, evidence for which is also seen in the Hα Fabry-Perot maps at smaller radii.

These observations show the power of sensitive H I and deep optical imaging of peculiar systems. It has long been believed that Arp 299 is in a very early stage of its interaction, given the relative youth of the on-going starburst ($\lesssim$20 Myr; Vacca *et al.* in preparation; Meurer *et al.* 1995; Stanford 1989; Nakagawa *et al.* 1989; Augarde & Lequeux 1985). The apparent lack of tidal features in their H I observations led Standford & Wood (1989) to conclude that the outer tidal H I had quickly settled into a disk configuration early in the encounter. The discovery of the 180 kpc tidal tail obviously changes this conclusion. It also requires the interaction to be quite old. Taking a typical rotation speed of 240 km s^{-1} from the inner disk kinematics and saying that this is the maximum velocity available to the tidal debris, we calculate that the tail has taken at least 750 Myr to form. Therefore *the dynamical age of the merger is substantially larger than the age of the present starburst.* Arp 299 is not unique in this sense (e.g. Mihos & Bothun 1998), and this cautions against using the age of the starbursts to age-date an interacting system, as is frequently done for the peculiar star-bursting objects at high redshift. Further, it is possible that Arp 299 experienced several short bursts of elevated star formation since the tail was first launched. In this case, the accumulated burst populations would not be co-eval, but would show a spread of ages, and the expected age signatures in the resulting remnant will be much less pronounced then is often presumed (*e.g.* Silva & Bothun 1998).

4.2. *The Nature of the Progenitors*

Now that we have used the H I kinematics to approximately associate the different kinematic features and their progenitors, we attempt to divide the gas content and B-band luminosities between the two systems. We will then use these global quantities in concert with the statistical properties of normal Hubble types in an attempt to deduce the approximate Hubble types of the progenitors. It should be noted that not only are there significant uncertainties inherent in apportioning the gas and light between the two systems, but there is also a notoriously large scatter in global properties along the Hubble sequence, and a further uncertainty due to conversion between gas phases and from gas into stars due to the on-going starburst. However the following should provide a very rough guess for the likely progenitors.

As mentioned above, we associate the H I from the tidal tail and minor axis clump with NGC 3690 (M_{HI}=3.5$\times$10$^9 M_\odot$), and the inner disk and W plume of H I with IC 694 (M_{HI}=6.2$\times$10$^9 M_\odot$). Simple dynamics suggest that less than one-half of the disk can be ejected into a tidal tail, and that most of this quickly falls back onto the merging system (Hibbard & Mihos 1995). This suggests a total H I content of 2–3 $\times M_{HI,tidal}$ = (7–10)$\times$10$^9 M_\odot$ for NGC 3690. However, this value is already more than the combination of the tidal H I and the absorption correction (5.7$\times$10$^9 M_\odot$). This discrepancy suggests that our absorption correction was probably too conservative (§3.4). Rather than trying to account for gas that we have no firm measure of, we simply associate all of the absorption corrected gas (2.2$\times$10$^9 M_\odot$) with NGC 3690 and remark that the H I masses for both IC 694 and NGC 3690 are likely significantly underestimated. Using the $12CO(1-0)$ observations of Casoli *et al.* (1999), we associate the "widespread" molecular gas and that near source **A** with IC 694, the molecular gas near source **B** with NGC 3690, and split the molecular gas from the overlap region (**C-C′**) between the two systems. Total gas masses are calculated by adding the atomic and molecular hydrogen gas masses and multiplying by 1.36 to account for He. Finally, the individual B-band luminosities are estimated by summing the light over irregular polygons drawn around each system, and are therefore also very approximate. The results of this division are given in Table 4, and we use these values in concert with the following statistical properties of normal Hubble types:

- M_{H_2}/M_{HI} increases towards earlier Hubble types (Young & Knezek 1989, Young & Scoville 1991). The high values in Table 4 suggests progenitor types later than Sab and earlier than Sc. They also argue against low surface brightness progenitors (de Blok & van der Hulst 1998)
- M_{HI}/L_B increases towards later Hubble types (Roberts & Haynes 1994; Giovanelli & Haynes 1990). The high values in Table 4 suggest types later than Sa (Wardle & Knapp 1986, Bregman *et al.* 1992), and later than Sb (Roberts & Haynes 1994).
- The large mass of H I suggests types later than Sa (Huchtmeier & Richter 1988; Bregman *et al.* 1992) and earlier than Sc (Huchtmeier & Richter 1988; Giovanelli & Haynes 1990).
- The large values of M_{H_2} and M_{gas}/L_B suggest types later than Sa (Hogg *et al.* 1993).
- The large values of M_{H_2}/L_B favor types later than Sab (Lees *et al.* 1991, Bregman *et al.* 1992).

These consideration suggest progenitor types of Sab-Sc for both systems – an earlier type for IC 694 and a later type for the NGC 3690. This view is supported by high-resolution (1″) NIR imaging of the brightest sources at 2.2 μm by Wynn-Williams *et al.* (1991). In that study, the light profiles of the brightest NIR sources within Arp 299 were compared with stellar profiles taken immediately before and after the on-source exposures. It was found that source **A** is clearly resolved, with a FWHM of 460 pc (correcting to our adopted distance of 48 Mpc), while the point sources within NGC 3690 are found to have cores that are indistinguishable from stars, implying that they have diameters of less than 230 pc at 2.2μm. These considerations suggest a more extended bulge for IC 694 than for NGC 3690, lending further support to an earlier type for the former and a later type for the latter. We therefore suggest progenitor types of Sab-Sb for IC 694 and Sbc-Sc for NGC 3690.

In summary, we believe that Arp 299 results from a prograde-retrograde encounter between a gas-rich Sab-Sb (IC 694) and Sbc-Sc (NGC 3690) that occurred 750 Myr ago. We estimate that the system will fully merge on a timescale somewhere between a crossing time (d/v_{max}) and an orbital period ($\pi d/v_{max}$) at the present separation d of 4.7 kpc, or sometime between 20–60 Myr from now (for a rotational speed of 240 km s^{-1}).

4.3. *Explanations for Outer Tidal Morphology*

The differences between the gaseous and stellar tidal morphologies were very unexpected. Displacements between optical and gaseous tails or bridges are not unheard of (e.g. NGC 4725/47, Wevers *et al.* 1984; Arp 295, HvG96; NGC 7714/5, Smith *et al.* 1997; NGC 2782, Smith 1994); nor are gaseous tidal tails or streamers with little, if any, starlight (e.g. NGC 2444/5, Appleton *et al.* 1987; M81, Yun *et al.* 1994); nor are stellar tails or plumes with no H I (e.g. NGC 3921, HvG96; Arp 105, Duc *et al.* 1997; NGC 2782, Smith 1994). There are even examples of much less extreme "bifurcated" gaseous tails, in which a single tidal tail appears to split near its base into parallel H I filaments, both of which have similar kinematics (e.g. M81 Yun *et al.* 1994; NGC 3921 HvG96; NGC 2535/6 Kaufman *et al.* 1997; NGC 4038 Hibbard, van der Hulst & Barnes, in preparation). What is unique in Arp 299 is that all these effects occur at once — there is a tail which is bifurcated along almost its entire length, with one filament gas rich and the other gas poor, and a striking anti-correlation between the gaseous and stellar filaments where the filaments join. In this subsection, we investigate possible explanations for each of these characteristics in turn.

4.3.1. *Gas-Rich Outer Filament*

The high M_{HI}/L_B ratios found for the outer filament are rather extreme, with peaks >10 $M_\odot\, L_\odot^{-1}$ and a mean of ∼4 $M_\odot\, L_\odot^{-1}$. However they are similar to the values found in other gaseous tidal extensions (e.g. Arp 143 Appleton *et al.* 1987; NGC 2782 Smith 1994; NGC 7252 Hibbard *et al.* 1994). In these systems, the gas-rich extensions appear to be due to the fact that M_{HI}/L_B is an increasing function of radius in spiral galaxies (Wevers *et al.* 1986)[10]. Since the outermost (gas-rich) regions of the disk become the outermost regions of the resulting tidal tails (TT72), gas rich extensions to optical tails are to be expected. The higher dispersion of outer disk stars with respect to the gas (van der Kruit 1988) and the finite lifetimes of the most luminous stars will exacerbate this effect, leading to further increases in M_{HI}/L_B in the outer regions (HvG96).

However, Arp 299 is quite different from the above mentioned systems in that it is not just the outermost regions that are gas rich — the gas-rich filament appears to extend all the way back to the main body, running parallel to the optical tail. That is, it appears to cover a very broad range of radii. So the first question we wish to address is whether such a feature can arise due to a combination of dynamical and projection effects which cause the gas-rich outer regions to be projected adjacent to the optically brighter inner regions.

We believe that answer to this question lies in the dynamical development of tidal tails, as demonstrated so vividly by TT72. These authors emphasized that tails are not linear structures, but actually two dimensional "ribbons" twisting through space. In particular, Fig. 2 of TT72 shows that the outermost edges of the ribbon come from the outermost radii of the original disk, while middle regions come from intermediate radii, etc.; hence, the outer disk material forms a "sheath" around the inner disk material along its entire length. Therefore it is possible that a lateral twist may cause the outer edge of the ribbon to lie in a different plane from the inner regions, i.e. for the most gas-rich regions to appear in a different plane from the less gas-rich, optically brighter regions.

[10]This is usually expressed as the well-known fact that H I disks often extend further than optical disks e.g. Bosma 1981, Wevers *et al.* 1986, Cayatte *et al.* 1994, Broeils & van Woerden 1994.

The models also show that the material from different radii form continuous structures in space and velocity, and hence that the resulting tidal features will necessarily be continuous in space and velocity as well (Barnes 1988, Hibbard & Mihos 1995). But while the parallel filaments of Arp 299 appear to be kinematically continuous, they appear morphologically distinct, or bifurcated. We suggest that the bifurcation arises due to a pre-existing warp in the outer regions of one of the disk. This suggestion comes from our recent attempts to match the tidal morphology and kinematics of the northern tail using N-body simulations (Hibbard *et al.* in preparation). In our preliminary trials (using only 4096 particles per galaxy), we can rather easily match either the morphology and kinematics of the outer tidal filament and N clump, or the kinematics of the inner filament and morphology of the stellar tail. However we have been unable to match both features simultaneously with a single disk orientation and viewing angle. This leads us to suspect that the disk of NGC 3690 was initially warped (as is often the case for disk galaxies; Bosma 1991). In this case, the outer, optically fainter regions will be pulled off along one plane (resulting in the outer tidal filament), while the regions from smaller radii will move primarily in a different plane (resulting in the inner filament). A similar explanation may account for the less extreme bifurcated structures seen in other tidal tails (e.g. M81 Yun *et al.* 1994; NGC 3921 HvG96; NGC 2535/6 Kaufman *et al.* 1997; NGC 4038 Hibbard, van der Hulst & Barnes, in preparation).

However, this projection effect does not explain the low H I content of the optical tail in Arp 299. Although the less extreme radii of spirals have a lower M_{HI}/L_B than the outer regions, they still have significant quantities of H I. We therefore seek a separate explanation for this feature.

4.3.2. *Gas-Poor Inner Filament*

For the original disk to simultaneously give rise to a gas-rich outer filament and a gas-poor optical filament would require a special H I radial distribution — one in which the gaseous disk had a low column density within the stellar disk, but was very gas-rich beyond this. Such distributions are indeed seen in some early type galaxies, especially SB0's (van Driel & van Woerden 1991). However, two facts lead us to suspect that this is not a viable explanation for Arp 299. The first is that such systems usually have an order of magnitude less H I than observed in the tidal tail of Arp 299 (which itself is less than half of the original gas content). The second is that the starlight in such systems is dominated by an extended central bulge, which the NIR observations appear to rule out for NGC 3690 (§4.1).

Another factor that leads us to consider other explanations is that Arp 299 is one of a number of peculiar starburst galaxies exhibiting curious displacements between tidal H I and starlight. Further, the five systems which exhibit the most dramatic displacements (M82, Yun *et al.* 1993; NGC 4631/4656, Weliachew *et al.* 1978; NGC 520, HvG96; Arp 220 Yun, Hibbard & Scoville in preparation, HVY99; and Arp 299) also host massive nuclear starbursts with associated powerful outflows that extend many kpc from the nuclear regions ("superwinds", e.g. Heckman, Lehnert & Armus 1993; Lehnert & Heckman 1996), and in each case the tidal H I shows a displacement or anti-correlation along the direction of the expanding hot superwind fluid. This leads us to suspect a possible interaction between the expanding wind fluid and the tidal debris (see also Chevalier & Clegg 1985; Yun *et al.* 1993; Heckman, Lehnert & Armus 1993; Dahlem *et al.* 1996).

This issue is covered in more detail in HVY99, and here we just discuss the specific details of Arp 299. In this system the evidence for an expanding superwind comes from the morphology and kinematics of the optical emission line gas (Armus, Heckman & Miley 1990) and the X-ray observations of Heckman *et al.* (1999). In the latter, the soft X-ray emission from hot gas is oriented perpendicular to the harder X-ray emission from discrete x-ray sources associated with the starburst. The hot gas emission is elongated roughly along the minor axis of IC 694, extending to a radius of order 25 kpc (Heckman *et al.* 1999). Since the observed X-ray emission represents just the hottest, densest portions of the adiabatically expanding wind (Wang 1995), the full extent of the wind should extend well beyond this.

The mechanical effect of such a wind may be evidenced in the increased column density and velocity dispersion of the H I knot in the inner filament ($r \approx 60$ kpc), which might be due to the winds ram-pressure effects. The wind might also account for the high-velocity envelope of gas seen in Fig. 9 and the high velocity dispersion regions seen on the southern end of the N clump in Fig. 7d. However, we do not believe that the winds ram pressure has pushed the gas fully out of the inner filament and into the outer filament. Such action should significantly change the kinematics of the gas, whereas the kinematics of the gas within both filaments are nearly identical. Instead, we suspect that the superwind affects the ionization state of the gas in one of two ways: either directly by shock ionization, or indirectly by clearing a sight-line from the tidal tail to the nuclear starburst, allowing UV photons from the young stars to escape these regions and reach parts of the tail. Calculations carried out in HVY99 suggests that both scenarios are in principle capable of affecting gas at the observed column densities and distances, although there is insufficient evidence to discriminate between them.

Whether the "missing" H I has been ionized or not is subject to observational investigation. The expected emission measure in convienient units is $EM = 0.42\,\mathrm{cm}^{-6}\,\mathrm{pc}\,(\frac{N_{HI}}{2\times10^{20}\,\mathrm{cm}^{-2}})^2(\frac{10\,\mathrm{kpc}}{dL})^2$, where N_{HI} is the missing column density of H I, and dL is the line-of-sight depth of the H I column. If the gas has a clumpier distribution, then there should be some higher density peaks with emission measures well above these levels. These emmission measures are within the capabilities of modern CCD detectors (e.g. Donahue *et al.* 1995 obtained 0.3 cm^{-6} pc in NGC 4631), and such emission would be well worth looking for.

4.3.3. *Gas/Light Anti-correlation in the N Clump*

The main problem with the above scenarios is that neither can explain the H I and optical anti-correlation at the end of Arp 299 tail, whereby there is a local minima in the H I column density where the optical tail crosses the N Clump, and local maxima to either side of this (Fig. 7b). The expanding galactic wind or photoionization cone should have no idea where the optical tail lies.

In HVY99, we suggest that the outer H I from the warped disk is already in a highly ionized phase, due to its low density and the intergalactic UV field. In this environment, we suggest that the additional ionizing radiation due to evolved sources within the stellar tail itself, such as late B stars and/or white dwarfs, increases the ionization fraction of the local gas over that of the tidal gas without accompanying starlight. The lower neutral fraction is then seen as a drop in the neutral gas column density. A simple calculation is carried out in HVY99 that suggests that this process is in principle feasible, if the gas in the N clump has a line-of-sight thickness $\gtrsim$25 kpc. In thise case, the expected emission measure ($\lesssim$0.02 cm^{-6} pc) is well below what is observable with current technology.

4.3.4. *Outer morphology: conclusions*

These explanations are somewhat unsatisfactory since we need three separate mechanisms to explain the three puzzling characteristics: a warped H I disk to explain the parallel tidal filaments; a starburst wind or unusual initial H I distribution to explain the lack of H I within the optical filament; and an increased ionization fraction in the gas due to the presence of the stellar tail to explain the anti-correlation between the H I and optical light in the N clump. Whatever their cause, these observations point to some important differences occurring between gas and stars during the formation of some tidal tails.

4.4. *Conditions for Luminous Infrared Phase*

A main objective of our studies on the atomic gas in IR luminous galaxies ($L_{IR} > 3{\times}10^{11} L_\odot$, Hibbard & Yun 1996 and in preparation) and the molecular gas in the less-IR luminous systems of the Toomre Sequence (Yun & Hibbard 1999) is to investigate the conditions necessary for fueling a highly elevated period of star formation. Certainly a high gas content is one of the pre-requisites for fueling such large starbursts (Sanders *et al.* 1988). We are interested in knowing whether all mergers between gas rich galaxies pass through such a phase, or if there are requirements on the progenitor properties or encounter characteristics to trigger such bursts. To gain some insight into how this efficient mode of star formation is triggered in Arp 299, we draw upon statistical studies of luminous IR galaxies and the results of numerical simulations.

The tight correlation between molecular gas column density (Σ_{H2}) and L_{IR}, especially when compared with the much looser correlation of gas mass with L_{IR}, shows that IR luminous starbursts are always precipitated by a corresponding increase in the nuclear column densities of molecular gas (Scoville *et al.* 1994; Solomon *et al.* 1997; Kennicutt 1998; Taniguchi & Ohyama 1998; Yun & Hibbard 1999). The CO observations of Arp 299 (Sargent & Scoville 1991, Aalto *et al.* 1997, Casoli *et al.* 1999) show that the highest column densities in Arp 299 occur at the nucleus of IC 694, with Σ_{H2} over three times higher than at the nucleus of NGC 3690. Additionally, HCN mapping observations of Arp 299 (Aalto *et al.* 1997, Casoli *et al.* 1999) shows that the vast majority of the very dense gas ($n > 10^4\,\mathrm{cm}^{-3}$) is associated with the nucleus of IC 694.

Since the two progenitor galaxies appear to be of nearly equal mass and of similar total gas content (Table 4), we suggest that the reason there has been so much more gaseous dissipation towards the nucleus of IC 694 is due to its retrograde spin geometry (see also Sanders *et al.* 1988). In such encounters, the gas within the disk is not pulled into tidal bridges and tails, but rather remains in the disk where it feels the perturbation from the second system alternately pulling it outward and pushing it inward during an orbit (e.g. TT72; White 1979; Noguchi 1991). This excites large epicyclic motions in the gas, which in turn leads to higher collision rates (e.g. Olson & Kwan 1990; Noguchi 1991) and hence to more gaseous dissipation.

This suggestion would seem to be at odds with the results from numerical simulations, which find only a moderate dependence of gaseous dissipation and/or starformation activity on the encounter spin geometry (e.g. Mihos & Hernquist 1996; Barnes & Hernquist 1996). Further, these simulations invariably have the starbursts occurring only when the nuclei finally coalesce, while in Arp 299 (and other IR luminous mergers, Murphy *et al.* 1996, Mihos & Bothun 1998), the nuclei are still well separated ($d > 4.7$ kpc). A possible solution to these concerns is found in the simulations of Noguchi (1991), who stresses the episodic nature of starbursts in mergers (see also Olson & Kwan 1990). Noguchi notes that while the maximum enhancement of activity is not strongly dependent on the spin geometry of the encounter, the time evolution of the activity is. In particular, his prograde-retrograde encounter produces a longer period of enhanced activity over other spin combinations and also leads to a slower coalescence of the nuclei. As a result, the cloud collision rate is still significantly increased as the nuclei separate (see his Fig. 9). This model predicts that the most luminous phase of Arp 299's starburst is still in the future, in which case this merger is predicted to out-shine even Arp 220.

However, the numerical simulations are necessarily adhoc in nature, and the micro-physics of hydrodynamics (e.g. SPH as in Mihos & Hernquist and Barnes & Hernquist vs. sticky particle as in Noguchi), star formation, and "feedback" (energy input back into the interstellar medium due to star formation) is poorly understood. Therefore, before drawing too many inference from the simulations, it would be prudent to first test the numerical formalisms for star formation, dissipation, and feedback by direct comparison with real systems. Until simulations can reproduce starbursts occurring at the times and locations as observed, we must be cautious when extrapolating their results too far into the future.

The *observational* fact that systems can experience much of their star formation when the nuclei are well separated has important ramifications for the structure of the resulting remnant. In particular, stars are dissipationless and cannot radiate their orbital energy away. Therefore stars that form while the nuclei are well separated will be spread over a larger range of radii in the resulting remnant than those that form when the nuclei are practically merged. This population can experience violent relaxation (e.g. Barnes 1992; Barnes & Hernquist 1996), resulting in an extended dynamically hot population. The resulting remnant will have a much more regular luminosity profile than a merger in which the gas all sinks to the very center of the potential before forming stars (*cf.* concerns raised in Mihos & Hernquist 1994).

4.5. *Lack of Tidal Dwarfs*

The widespread lack of small-scale correlation between optical and gaseous density enhancements within the tidal tail was unexpected. In previous H I and optical observations of six double-tailed merging systems (van der Hulst 1979; Hibbard & van Gorkom 1993, 1996; Hibbard *et al.* 1994), five dwarf galaxy like concentrations of gas, light and Hα emission appear entrained within tidal tails *and* coincident with distinct features in the optical color maps and the H I velocity dispersion maps. These concentrations have been interpreted as "tidal dwarf galaxies" forming out of the expanding tidal material (see also Schweitzer 1978; Mirabel, Dottori & Lutz 1992; Duc *et al.* 1997; Malphrus *et al.* 1997), an idea that has been supported by numerical simulations (Barnes & Hernquist 1992, 1996; Elmegreen, Kaufmann & Thomasson 1992; Hibbard & Mihos 1995). In addition to these dwarf-sized concentrations, the previously observed tidal tails often contain numerous knots of gas, light, and star-forming regions (see also Hutchings 1996; Hunsberger, Charlton & Zaritski 1996; Mihos & Bothun 1998). We therefore fully expected similar features to appear in a tidal feature as long and as massive as that seen in Arp 299.

However, the optical tail of Arp 299 is remarkably smooth and featureless (Fig. 5). There are a number of point sources falling upon the optical tail, but the surface density of such points is similar to that of point source elsewhere in the field. Their colors are generally quite red ($B-R > 1.7$, Fig. 7a), and most are probably background galaxies. And while there is considerable structure within the H I tail, there are no H I peaks with a corresponding enhancement in the underlying starlight (Fig. 7b). Further, there are only three regions which exhibits a significant (>20%) increase in the H I velocity linewidth (indicated in Fig. 7d) — along the southern edge of the N clump and at the H I knot in the inner tidal filament (§3.3) — and these features do not correspond to any notable features in the optical images or color maps.

To further investigate this question, we estimate the importance of self-gravity within the tail by comparing the luminous mass (M_{lum}) to the dynamical mass (M_{dyn}). The luminous mass is estimated by adding the gas mass and the stellar mass. The latter is estimated from the B-band surface brightness and adopting a stellar mass to light ratio of $(M/L)_B = 2M_\odot L_\odot^{-1}$, characteristic of stellar disks (Bottema 1993). The dynamical mass is calculated via $M_{dyn} = 1.76 \times 10^6 M_\odot \times \sigma_{HI}^2 \times r_{1/2}$ (Binney & Tremain 1987; see also Kaufman *et al.* 1997), where $r_{1/2}$ is the FWHM radius of the beam (~ 1.9 kpc for the high resolution data). This will over-estimate the effects of self-gravity if (1) the line-of-sight dimension of the tail is larger than the beam width (~ 3.8 kpc), in which case the above prescription overestimates the stellar mass; and if (2) the stars contribute significantly to M_{lum} and have a velocity dispersion greater than σ_{HI} (e.g. van der Kruit 1988). Since we suspect both of these conditions to hold, our calculation of M_{lum}/M_{dyn} should be a stringent upper-limit. We derive a lower limit to M_{lum}/M_{dyn} by setting $M_{lum} = M_{gas}$.

Using the high resolution data, we find that $M_{lum}/M_{dyn} < 0.3$ everywhere, with the highest values on the brighter optical peaks of the inner tidal filament[11]. The peaks in the H I column density along the outer filament and in the N clump have $0.2 < M_{lum}/M_{dyn} < 0.3$, and the H I knot in the inner filament has $0.1 < M_{lum}/M_{dyn} < 0.2$. For comparison, the tidal dwarfs in the tail of NGC 7252 (Hibbard *et al.* 1994), NGC 3921 (Hibbard & van Gorkom 1993, HvG96) and NGC 4038/9 (Mirabel, Dottori & Lutz 1992) have $0.50 \lesssim M_{lum}/M_{dyn} \lesssim 1$. Therefore Arp 299 lacks the potentially self-gravitating dwarf-like concentrations seen in other tailed systems, and we conclude that tidal dwarf formation is not a ubiquitous process.

This suggests that the formation of such sub-structures may depend on factors other than the ability to raise a decent sized tail. We note that other tidal tails which contain candidate tidal dwarf galaxies have similar gas column densities as in the tail of Arp 299, but have optical tails that are $\sim$2 mag arcsec^{-2} brighter. Additionally, in these systems the gas and optical material coincide. Both of these factors increasing the underlying mass density within the tail. Further, since the gas in observed tidal dwarfs are a significant contribution to the dynamical mass ($M_{gas}/M_{dyn} \approx 0.5$), it may be the case that whatever process removes the H I from the inner tidal filament (see §4.3.2) also suspends the dwarf formation process.

Whatever the explanation, the present observations suggest that one should be cautions about simply measuring the mass or light contained within the highest gas column density contours or optical isophotes and calling these concentrations distinct entities.

5. CONCLUSIONS

- A new tidal tail has been discovered in the on-going merger Arp 299. The tail stretches 180 kpc to the north, and must have taken at least 750 Myr to form. This is much longer than the age of the current starburst, suggesting that the starburst and merger clocks start at different times and run at different rates. If the present starburst began when the tidal tail was first launched, the spread of ages in the resulting remnant will be much larger than is usually assumed.

- What had previously been interpreted as a single rotating gaseous disk surrounding the two merging systems is shown to be a gaseous disk associated with the eastern system, IC 694. The kinematic information in concert with the optical morphology allows us to deduce that NGC 3690 experienced a prograde encounter while IC 694 experienced a retrograde encounter. From the cold gas contents and NIR morphologies, we suggest late type progenitors for both systems (Sab-Sb for IC 694, Sbc-Sc for NGC 3690).

- The observations show that Arp 299 is experiencing an IR bright starbursts while the nuclei are still well separated ($dr \gtrsim 4.7$ kpc). We suggest that this is due in part to the retrograde spin geometry of IC 694.

- The tidal morphology is unique among mergers: there is a low surface brightness stellar tail with low column density H I and a conspicuous parallel gaseous tail of higher H I column density and with

[11] Using a velocity dispersion of 20 km s^{-1} as inferred for the stars in §3.2 would give $M_{lum}/M_{dyn} < 0.04$ on this feature

little, if any, associated starlight. The tails have very similar kinematics suggesting that they are physically connected. We suggest that such bifurcated or parallel tails result from a progenitor with a warped disk. However, this explanation does not explain the low H I content of the optical tail.

- The similarity between this tidal morphology and that of other starburst galaxies with direct evidence of superwind outflows (M82, NGC 4631, NGC 520, Arp 220) suggest that the galactic superwind recently imaged by Heckman *et al.* (1999) may be responsible for clearing the optical tail of much of its cold diffuse gas. Local ionizing sources within the tidal tails may also play a role in some of the observed optical/gaseous anti-correlation. These issues are explored in more detail in HVY99
- The absence of dwarf galaxy-like mass concentrations in the tidal tail suggests that tidal dwarf formation is not a ubiquitous process. It is possible that the whatever process removed gas from the optical tail may have consequently suppressed the dwarf formation process.

We would like to thank S. Aalto, L. Armus, F. Casoli & F. Combes for sharing of data and information prior to publication. We thank the referee, Tim Heckman, for a timely and useful referees report which helped clarify many areas of this paper. JEH would like to thank the Owens Valley group at Caltech, and in particular Nick Scoville, for the hospitality extended during the summer of 1995 to reduce the H I data presented in this paper. Thanks also to W. Vacca, J. van Gorkom, J. Barnes and G. Stinson for useful conversations. JEH acknowledges support by Grant HF–1059.01–94A from the Space Telescope Science Institute, which is operated by the Association of Universities for Research in Astronomy, Inc., under NASA contract NAS5–26555, for much of this research.

Most of the figures in this paper were made with the WIP interactive software package (Morgan 1995). This research has made extensive use of the NASA/ IPAC Extragalactic Database (NED), which is operated by the Jet Propulsion Laboratory, California Institute of Technology, under contract with the National Aeronautics and Space Administration. The Digitized Sky Surveys were produced at the Space Telescope Science Institute under U.S. Government grant NAG W-2166. The images of these surveys are based on photographic data obtained using the Oschin Schmidt Telescope on Palomar Mountain and the UK Schmidt Telescope. The plates were processed into the present compressed digital form with the permission of these institutions.

APPENDIX

WHO IS IC 694?

There is some confusion in the printed and electronic literature as to which systems actually comprise Arp 299 (e.g. IAU circular 6859; NED)[12]. Arp does not offer many clues, and even confuses the matter by incorrectly designating Arp 296 as NGC 3690+IC 694 in Tables 1 & 2 of his Atlas, while giving Arp 299 no further designation (Arp 1966). However the description in Arp's Table 1, and the order of his figures (Arp 296 appearing next to other bridge-tail systems) makes it clear that Arp published the pictures under the correct number, and gave them the correct description in Table 1, and just got the "Designation" switched in both tables.

The description given for NGC 3690 in the NGC (Dreyer 1888) translates as "pretty bright, pretty small, very little extended at PA=80, pretty gradually brighter towards the middle, small stars south following near". According to the NGC "pretty small" means a diameter of $50''$-$60''$, and this radius would incorporate much of the brighter parts of the system (including the nucleus of the eastern system). Given that the five highest surface brightness objects are within $7''$ of source **B** in the western system, through a small telescope this object must have looked like a single nucleus at the location of source **B** in Fig. 1 with a cloud of surrounding nebulosity, and it is unlikely that two nuclei could have been discerned. It therefore seems likely that the original designation refers to the entire Arp 299 system, although only one nucleus was identified (corresponding to the western system, what we have been calling NGC 3690 in the above). Therefore whether NGC 3690 should strictly apply to the entire system or to only the western system depends on if you believe galaxies are identified by their nuclei or their integrated light. We remain agnostic on this point, and from here investigate which object was designated as IC 694.

The earliest and clearest association of IC 694 with the eastern system can be traced to Vorontsov-Vel'yaminov, in his *Atlas and Catalogue of Interacting Galaxies* (Vorontsov-Vel'yaminov 1959), where Arp 299 appears as VV118a-e. Source VV118a is the galaxy to the East (what we have been referring to as IC 694), VV118b the system to the west (what we have been calling NGC 3690), VV118c is MCG+10-17-2a, the compact spheroidal $1'$ to the NW, and VV118d & e are bright HII regions in the outer disk to the NW. In the accompanying table to the Atlas, VV118a is identified as IC 694, VV118b is identified as NGC 3690, and sources c,d or e have no other designations. The vast majority of researchers since have followed this designation. Nilson first brings up the question of the identification of IC 694 with VV 118a in the UGC (Nilson 1973), in his notes on UGC 6471/2: "Arp 296 (identified as NGC 3690 + IC 694 by Arp) are faint objects north-preceding UGC 06471 + UGC 06472, magnitude approximately 17 and 21 identification of IC 694 uncertain, may be a small object north-preceding and inside the outer parts of the double system". [The use of the name Arp 296 is

[12]For this discussion, it is instructive to look at an earlier photographic representation of the Arp 299. For this, we refer to reader to Plate 1 of Morgan (1958). In this figure, the NW spheroidal appears as a very faint fuzz well separated from and much dimmer than either of the two interacting disks, which appear as distinct objects.

immediately attributed to Arp's error in making his tables, discussed above].

IC 694 was discovered by Swift (1893), whose discovery description translates as "close double with NGC 3690 = object 247 of list I of Sir William Herschel. Suspected at 132x magnification, verified at 200x". In the *Index Catalogue of Nebulae* (IC, Dreyer 1895) this becomes "very small, forms double nebula with no. 247 of list I of Sir William Herschel". "very small" translates as $10''$-$20''$ diameter, which is on the large side for the NW spheroidal ($\theta_{FWHM}\sim4''$). There is no definition of the term "double" in the IC[13], and perhaps this is where the confusion lies. Certainly with todays knowledge we would call Arp 299E+W a double, and the spheroidal to the NW a possible companion. However, is this how Dreyer and Swift used the term?

So the question is, when Swift identified IC 694, did he subdivide the NGC 3690 entry, or add an entry for the faint nebulosity to the NW? The position for IC 694 is given as 11:20:44 +59:20 (epoch 1860) in the IC, while the NGC position for NGC 3690 is 11:20:45 +59:19, *i.e. IC 694 lies approximately 1′ to the NW of NGC 3690.* This seems like pretty conclusive evidence that IC 694 indeed refers to the spheroidal to the NW. However, Dreyer remarks in the introduction to the IC that Swifts positions are "generally reliable within one or two minutes of arc, but larger errors occur occasionally..." We also learn from Dreyer that Swifts observations were taken through a $16''$ refractor at the Rochester Observatory. Since the NW galaxy is 3 mag fainter than either of the disk galaxies (m_B=16.2 mag from CCD observations reported above), is it even possible for Swift to have seen the NW companion? If not, it is likely that he simply resolved NGC 3690 into two separate condensations of nearly equal luminosity, adding a separate catalogue entry for the second system. A similar super-classification appears to have happened in the case of NGC 4861/IC 3961 (Arp 266) and NGC 2207/IC 2163.

Recent attempts to repeat these observations with similar sized telescopes by amateur astronomers suggest that (1) the second light concentration now associate with the nucleus of Arp 299E is very easy to discern as distinct from Arp 299W; and (2) the NW spheroidal is indeed a *very* difficult, but not an impossible, object. Combined with the correct relative position of IC 694 given by Swift, it seems that there is strong evidence that IC 694 properly designates the NW compact spheroidal. However, since these observations were made with prior knowledge of both the existence and location of the NW spheroidal, this confirmation is not entirely independent. Since it is nearly impossible to prove this issue conclusively one way or the other, we choose to follow the vast majority of researchers and use the designation introduced by Vorontsov-Vel'yaminov (1959), concluding as Sulentic & Tift (1973) that "Any further question as to which objects Dreyer was referring to can only be of historical interest".

JEH offers special thanks to Harold Corwin, Steve Gottleib, Malcom Thomson, Bill Vacca and Dennis Webb for many useful discussions on this issue.

REFERENCES

Aalto, S., Radford, S. J. E., Scoville, N. Z., & Sargent, A. I. 1997, ApJ, 475, L107
Aaronson, M. Huchra, J., Mould, J., Schechter, P. L. & Tully, R. B. 1982, ApJ, 258, 64
Alton, P. B., Trewhella, M., Davies, J. I., Evans, R., Bianchi, S., Gear, W., Thronson, H., Valentijn, E. & Witt, A. 1998, A&A, 335, 807
Anantharamaiah, K. R., Zhao, J.-H., Goss, W. M. & Viallefond, F. 1993, ApJ, 419, 585
Appleton, P. N., Ghigo, F. D, van Gorkom, J. H., Schombert, J. M., & Struck-Marcell, C. 1987, Nature, 330, 140
Armus, L., Heckman, T. M, & Miley, G. K. 1989, ApJ, 347, 727
Armus, L., Heckman, T. M, & Miley, G. K. 1990, ApJ, 364, 471
Arp, H. C. 1966, ApJS, 14, 1
Augarde, R., and Lequeux, J. 1985, A&A, 147, 273
Baan, W.A. 1985, Nature, 315, 26
Baan, W.A., & Haschick, A. 1990, ApJ, 364, 65 **(BH90)**
Barnes, J. E. 1988, ApJ, 331, 699
Barnes, J. E. 1992, ApJ, 393, 484
Barnes, J. E., & Hernquist, L. 1992, Nature, 360, 715
Barnes, J. E., & Hernquist, L. 1996, ApJ, 471, 115
Beck, S. C., Turner J. L. & Ho, P. T. P. 1990, ApJ, 349, 57
Binney, J., & Tremaine S. 1987, "Galactic Dynamics", (Princeton, Princeton University Press)
Bohlin, R. C., Savage, B. D. & Drake, J. F. 1978, ApJ, 224, 132
Bosma, A. 1981, AJ, 86, 1791
Bosma, A. 1991, in "Warped Disks and Inclined Rings around Galaxies", edited by S. Casertano, P. Sackett & F. Briggs (Cambridge Univ. Press, Cambridge), p. 181
Bottema, R. 1993, A&A, 275, 16
Bregman, J. N., Hogg, D. E., & Roberts, M. S. 1992, ApJ, 387, 484
Briggs, D.S. 1995, PhD. Thesis, New Mexico Inst. Mining & Technology
Broeils, A. H., & van Woerden, H. 1994, A&AS, 107, 129.
Bushouse, H. A. & Gallagher, J. S., III 1984, PASP, 96, 273
Carico, D. P., Sanders, D. B., Soifer, B. T., Matthews, K., & Neugebauer, G. 1990, AJ, 100, 70
Casoli, F., Combes, F., Augarde, R., Fign, P. & Martin, J. M. 1989, A&A, 224, 31
Casoli, F., Willaime, M.-C., Viallefond, F. & Gerin, M. 1999, A&A, 346, 663
Carral, P., Turner, J. L., & Ho, P. T. P. 1990, ApJ, 362, 434
Cayatte, V., van Gorkom, J. H., Balkowski, C., & Kotanyi, C. 1994, AJ, 107, 1003
Chevalier, R. A., & Clegg A. W. 1985, Nature, 317, 44
Condon, J. J., Condon, M. A., Gisler, G., & Puschell, J. J. 1982, ApJ, 252, 102
Condon, J. J., Helou, G., Sanders, D. B., & Soifer, B. T. 1990, ApJS, 73, 359
Condon, J. J., Huang, Z. -P, Yin, Q. F., & Thuan, T. X. 1991, ApJ, 378, 65
Dahlem, M., Heckman, T. M., Fabbiano, G., Lehnert, M. D., & Gilmore, D. 1996, ApJ, 461, 724
de Blok, W. J. G. & van der Hulst, J. M. 1998, A&A, 336, 49
Dickey, J. M. 1982, ApJ, 263, 87
Dickey, J. M., Brinks, E., & Puche, D. 1992, ApJ, 385, 501
Doherty, R.M., Puxley, P.J., Lumsden, S.L & Doyon, R. 1995, MNRAS, 277, 577
Donahue, M., Aldering, G., & Stocke, J. T. 1995, ApJ, 450, L45
Dreyer, J. L. E. 1888, Mem. RAS, 49, 1
Dreyer, J. L. E. 1895, Mem. RAS, 51, 185
van Driel, W., van Woerden, H. 1991, A&A, 243, 71
Duc, P. -A., Brinks, E., Wink, J. E., & Mirabel, I. F. 1997, A&A, 326, 537
Dudley, C. C. & Wynn-Williams, C. G. 1993, ApJ, 407, L65
Dudley, C. C. 1998, Ph.D. Thesis, University of Hawaii
Elmegreen, B., Kaufmann, M., & Thomasson, M. 1993, ApJ, 412, 90
Fairall, A.P. 1971, MNRAS, 153, 303
Gehrz, R.D., Sramek, R.A. & Weedman, D.W. 1983, ApJ, 267, 551
Giovanelli, R. & Haynes, M. P. 1990, in "Galactic & Extragalactic Radio Astronomy", editors G. L. Verschuur, K. I. Kellermann, (Springer, Berlin), p. 522
Gooch, R.E., 1995, in "Astronomical Data Analysis Software and Systems V", ASP Conf. Series vol. 101, edited by G.H. Jacoby & J. Barnes (ASP, San Francisco) p. 80-83

[13]Ironically, in the introduction to the IC Dreyer states "the system of abbreviated description ... has been in use so long that it is unnecessary to enter into a lengthy explanation of it.."

Heckman, T. M., Armus, L., Miley, G. K. 1990, ApJS, 74, 833
Heckman, T. M., Armus, L., Weaver, K. A. & Wang, J. 1999, ApJ, 517, 130
Heckman, T. M., Lehnert, M. & Armus, L. 1993, in "The Evolution of Galaxies and their Environment", edited by H. A. Thronson and J. M. Shull (Kluwer, Dordrecht), p. 455
Hibbard, J. E. 1995, Ph. D. Thesis, Columbia University
Hibbard, J. E., van Gorkom, J. H. 1993, in "The Globular Cluster–Galaxy Connection", ASP conf. series, Vol. 48, edited by G. H. Smith and J. P. Brodie (ASP, San Francisco), p. 619
Hibbard, J. E., & van Gorkom, J. H. 1996, AJ, 111, 655 **(HvG96)**
Hibbard, J. E., Guhathakurta, P., van Gorkom, J. H., & Schweizer, F. 1994, AJ, 107, 67
Hibbard, J. E., & Mihos, J. C. 1995, AJ, 110, 140
Hibbard, J.E., & Yun, M.S., 1996, in "Cold Gas at High Redshift", edited by M. Bremer, H. Rottgering, P. van der Werf & C.L. Carilli (Kluwer, Dordrecht), p. 47
Hibbard, J. E., Vacca & W. D., Yun, M. S 1999, AJ, submitted **(HVY99)**
Hilker, M., & Kissler-Patig, M. 1996, A&A, 314, 357
Hoffman, L. G., Salpeter, E. E., Farhat, B., Roos, T., Williams, H. & Helou, G. 1996, ApJS, 105, 269
Hogg, D. E., Roberts, M. S., & Sandage, A. 1993, AJ, 106, 907
Huchtmeier, W. K. & Richter, O. -G. 1988, A&A, 203, 237
van der Hulst, J. M. 1979, A&A, 155, 151
Hunsberger, S., Charlton, J., & Zaritsky, D. 1996, ApJ, 462, 50
Hutchings, J. B. 1996, AJ, 111, 712
Jones, T. J., Gehrz, R. D. & Smith 1990, AJ, 99, 1470
Jones, T. J., 1997, AJ, 114, 1393
de Jong, R. S. 1995, Ph.D. Thesis, University of Groningen
Joy, M., Lester, D.F., Harvey, P.M., Telesco, C.M., Decher, R., Rickard, L.J. & Bushouse, H. 1989, ApJ, 339, 100
Kalberla, P. M. W., Schwarz, U. J., Goss, W. M. 1985, A&A, 144, 27
Kaufman, M., Brinks, E., Elmegreen, D. M., Thomasson, M., Elmegreen, B. G., Struck, C. & Klaric, M. 1997, AJ, 114, 2323
Keel, W. C., Kennicutt, R. C. Jr., Hummel, E., van der Hulst, J. M. 1985, AJ, 90, 708
Kennicutt, R.B., Jr. 1998, ApJ, 498, 541
Kinney, A. L., Bohlin, R. C., Calzetti, D., Panagia, N., Wyse, R. F. G. 1993, ApJS, 86, 5
Kobulnicky, H. A. & Dickey, J. M. 1999, AJ, 117, 908
van der Kruit, P. C. 1988, A&A, 192, 117
Lançon, A., Rocca-Volmerang, B., & Thuan, T.X. 1996, A&AS, 115, 253
Landolt, A. U. 1983, AJ, 88, 439
Lees, J. F., Knapp, G. R., Rupen, M. P., Phillips, T. G. 1991, ApJ, 379, 117
Lehnert, M. D., & Heckman, T. M. 1996, ApJ, 462, 651
Malphrus, B. K., Simpson, C. E., Gottesman, S. T. & Hawarden, T. G. 1997, AJ, 114, 1427
Mazzarella, J. M., & Boroson, T. A. 1993, ApJS, 85, 27
Meurer, G. R., Heckman, T. M., Leitherer, C., Kinney, A., Robert, C., & Garnett, D. R. 1995, AJ, 110, 2665
Mihos, J. C. & Bothun, G. D. 1998, ApJ, 500, 619
Mihos, J. C., Hernquist, L. 1994, ApJ, 437, L47
Mihos, J. C., Hernquist, L. 1996, ApJ, 464, 641
Miles, J. W., Houck, J. R., Hayward, T. L., & Ashby, M. L. N. 1996, ApJ, 465, 191
Mirabel, I. F., Dottori, H., & Lutz, D. 1992, A&A, 256, L19
Morgan, W. W. 1958, PASP, 70, 364
Morgan, J. A. 1995, in *"Astronomical Data Analysis Software and Systems IV"*, PASP Conf Series 77, editors R. A. Shaw, H. E. Payne, and J. J. E. Hayes, p. 129
Murphy, T. W. Jr., Armus, L., Matthews, K., Soifer, B. T., Mazzarella, J. M., Shupe, D. L., Strauss, M. A., Neugebauer, G. 1996, AJ, 111, 1025
Nakagawa, T.N., Nagata, T., Geballe, T.R., Okuda, H., Shibai, H. & Matsuhara, H. 1989, ApJ, 340, 729
Nilson, P. 1973, *Uppsala General Catalogue of Galaxies*, Uppsala Obs. Ann. 6
Noguchi, M. 1991, MNRAS, 251, 360
Nordgren, T. E., Chengalur, J. N., Salpeter, E. E., & Terzian, Y. 1997, AJ, 114, 77
Olson, K. M. & Kwan, J. 1990, ApJ, 361, 426
Ridgeway, S.E., Wynn-Williams, C.G. & Becklin, E.E. 1994, ApJ, 428, 609
Rieke, G.H. 1988, ApJ, 331, L5
Roberts, M. S. & Haynes, M. P. 1994, ARA&A, 32, 115
Roberts, C. 1996, in *"The Interplay Between Massive Star Formation, The ISM, and Galaxy Evolution"*, Proc. of the 11th IAP Astrophysics meeting, editors D. Kunth, B. Guiderdoni, M. Heydari-Malayeri & T. X. Thuan, (Editions Frontieres) p. 371
Rupen, M. P. 1999, in *Synthesis Imaging in Radio Astronomy*, ASP Conf. Series vol. XXX, ed. G. B. Taylor, C. L. Carilli and R. A. Perley (ASP, San Francisco) in press
Sanders, D. B., Soifer, B. T., Elias, J. H., Madore, B. F., Matthews, K., Neugebauer, G., & Scoville, N. Z. 1988, ApJ, 325, 74
Sanders, D. B., Scoville, N. Z., & Soifer, B. T. 1991, ApJ, 370, 158
Sargent, A.I., Scoville, N.Z. 1991, ApJ, 366, L1
Sargent, W.L.W. 1972, ApJ, 173, 7
Schombert, J. M., Wallin, J. F., & Struck-Marcell, C. 1990, AJ, 99, 497
Schweizer, F. 1978, "The Structure and Properties of Nearby Galaxies", IAU Symp. No. 77, edited by E. M. Berkhuijsen and R. Wielebinski (Reidel, Dordrecht), p. 279
Scoville, N.Z., Hibbard, J.E., Yun, M.S., van Gorkom, J.H. 1994, "Mass Transfer Induced Activity in galaxies", ed. I. Shlosman (Cambridge University Press, Cambridge), p. 191
Shier, L.M., Rieke, M.J. & Rieke, G.H. 1996, ApJ, 470, 222
Silva, D. R. & Bothun, G. D. 1998, AJ, 116, 85
Smith, B. J., Struck, C., & Pogge, R. W. 1997, ApJ, 483, 754
Smith, B. J. 1994, AJ, 107, 1695
Smith, D. A., Herter, T., Haynes, M. P., Beichman, C. A., & Gautier, T. N. 1996, ApJS, 104, 217
Smith, H.E., Lonsdale, C.J., & Lonsdale, C. J. 1998, ApJ, 492, 137
Solomon, P.M., Downes, D., Radford, S.J.E., & Barrett, J.W. 1997, ApJ, 478, 144
Stanford, S.A. 1989, ApSS, 157, 117
Stanford, S.A. & Wood, D.O.S. 1989, ApJ, 346, 712
Sulentic, J. W. & Tift, W. G. 1973, *The Revised New General Catalogue of Nonstellar Astronmical Objects*, (University of Arizona Press, Tucson)
Swift, L., 1893, MNRAS, 53, 273
Taff, L. G., Lattanzi, M. G., Bucciarelli, B., Gilmozzi, R., McLean, B. J., Jenkner, H., Laidler, V. G., Lasker, B. M., Shara, M. M. & Sturch, C. R. 1990, ApJ, 353, L45
Taniguchi, Y., & Ohyama, Y. 1998, ApJ, 509, L89
Telesco, C. M., Decher, R. & Gatley, I. 1985, ApJ, 299, 896
Toomre, A., & Toomre, J. 1972, ApJ, 178, 623 **(TT72)**
Tully, R. B. 1988, *Nearby Galaxy Catalog*, (Cambridge University Press, Cambridge)
Vorontsov-Vel'yaminov, B. A. 1959, "Atlas and Catalogue of Interacting Galaxies" (Moscow).
Wang, B. 1995, ApJ, 444, 590
Wardle, M., & Knapp, G. R. 1986, AJ, 91, 23
Weliachew, L., Sancisi, R., & Guelin, M. 1978, A&A, 65, 37
Wevers, B. H. M. R., van der Kruit, P. C., & Allen, R. J. 1986, A&AS, 66, 505
Wevers, B. H. M. R., Appleton, P. N., Davies, R. D., & Hart, L. 1984, A&A, 140, 125
White, S. D. M. 1979, MNRAS, 189, 831
Witt, A. N., Thronson, H. A. & Capuano, J. M. Jr. 1992, ApJ, 393, 611
Wynn-Williams, C.G., Eales, S.A., Becklin, E.E., Hodapp, K.-W., Joseph, R.D., McLean, I.S., Simons, D.A. & Wright, G.S. 1991, ApJ, 377, 426
Young, J. S., Knezek, P. M. 1989, ApJ, 347, L55
Young, J. S., & Scoville, N. Z. 1991, ARAA, 29, 581
Yun, M. S. & Hibbard, J. E. 1999, ApJ, submitted
Yun, M. S., Ho, P. T. P., & Lo, K. Y. 1993, ApJ, 411, L17
Yun, M. S., Ho, P. T. P., & Lo, K. Y. 1994, Nature, 372, 530
van Zee, L., Haynes, M. P., & Salzer, J.J. 1997, AJ, 114, 2497
Zezas, A. L., Georgantopoulos, I. & Ward, M. J. 1998, MNRAS, 301, 915
Zhao, J-H., Anantharamaiah, K.R., Goss, W.M., & Viallefond, F. 1997, ApJ, 482, 186

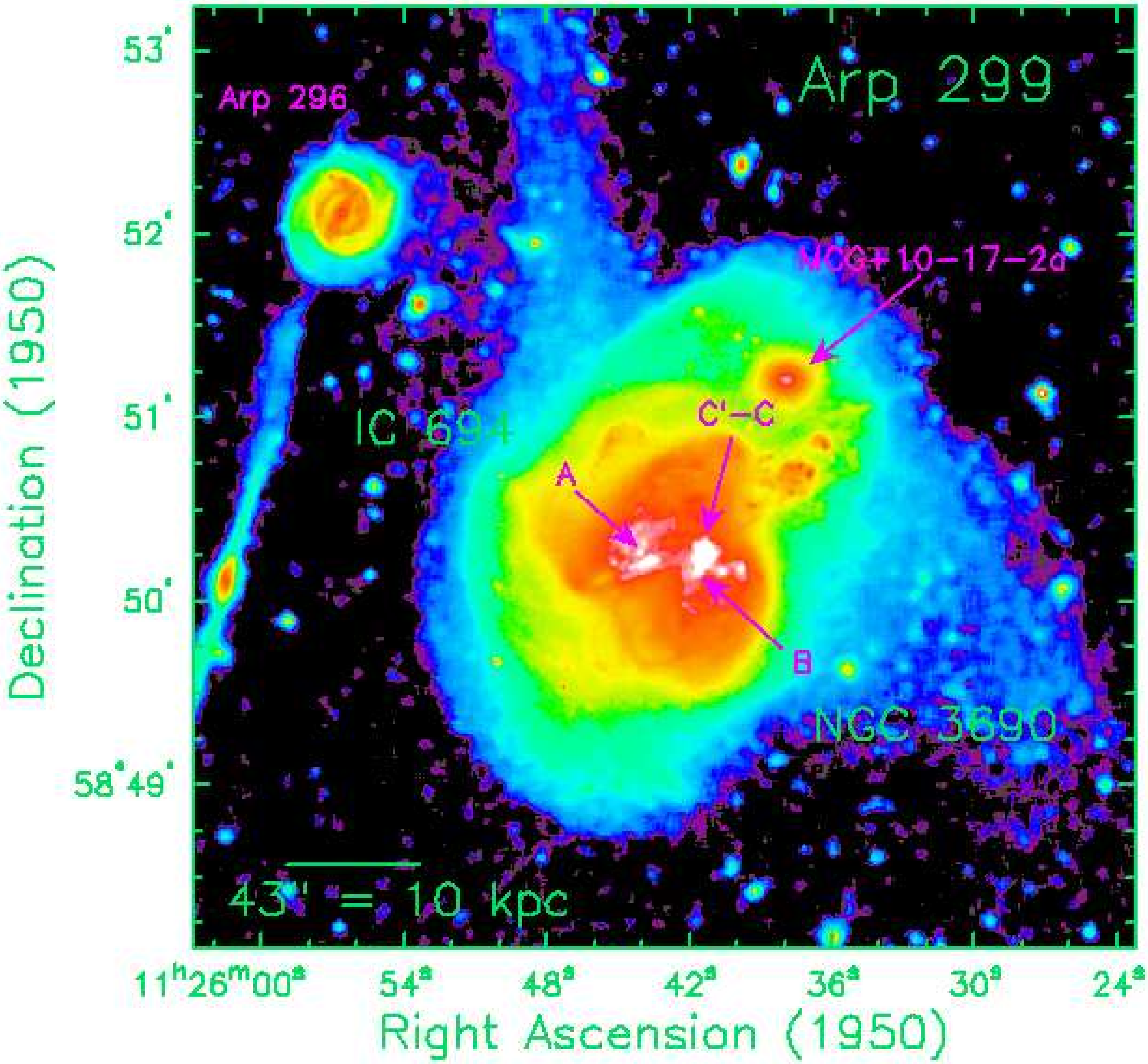

FIG. 1.— B-band image of the Arp 299 system. The optical image is displayed with a logarithmic transfer function, with white set to 28.5 mag arcsec^{-2} and black set to 22.75 mag arcsec^{-2}. IC 694 is to the left (east) and NGC 3690 is to the right, and north is up. Regions denoted as A,B, and C-C′ by Gehrz, Sramek & Weedman (1983) are so labelled. We also identify the associated system MCG+10-17-2a and the unrelated background bar/bridge/tail system Arp 296. A scale bar is drawn indicating 10 kpc, assuming a distance of 48 Mpc to Arp 299. The putative nuclei of the progenitors, as judge by NIR imaging and spectroscopy, are at regions A and B. Both of these locations are the sites of very dense molecular gas concentrations. The label C-C′ indicates the region of disk overlap, which is also the site of a significant concentration of molecular gas.

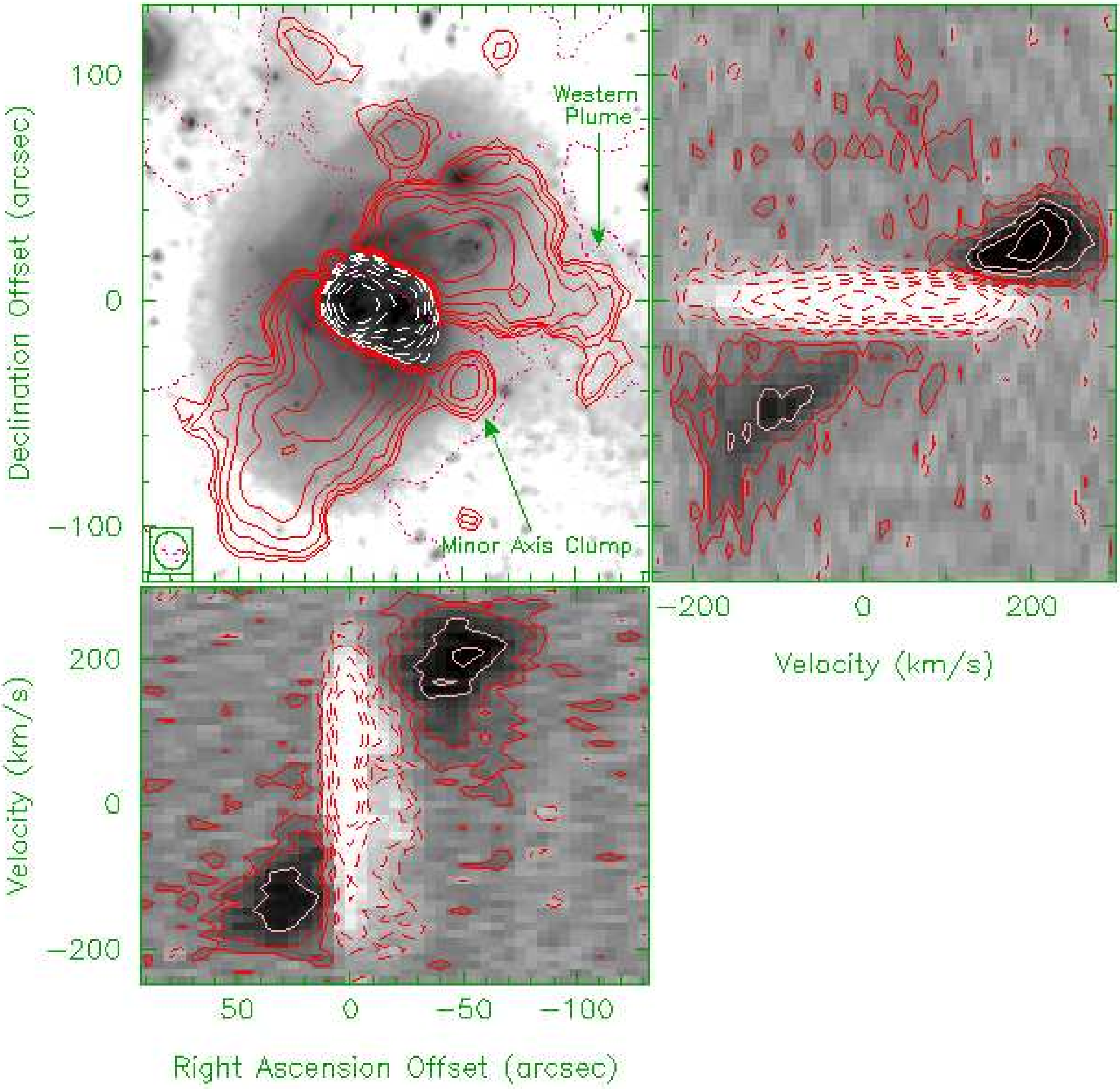

FIG. 2.— Position-Velocity profiles of the inner regions of Arp 299, demonstrating the kinematics of the inner H I features. The top left panel presents the B-band image displayed as in Fig. 1, with contours from the high resolution H I integrated intensity map superimposed (FWHM=17″×15″, as indicated by the ellipse in the lower left corner of the panel). Negative contours are drawn as dotted white lines, indicating the region of H I absorption. The positive contours begin at 11.05 mJy beam^{-1} km s^{-1} (5×10^{19}cm^{-2}), while negative contours begin at -33.15 mJy beam^{-1} km s^{-1}. Successive contour levels are twice the previous level. The black dotted contour indicates a column density of 1×10^{19}cm^{-2} from the low-resolution H I data (θ_{FWHM}=35″). To the right is a position-velocity map of the high resolution data after summing the emission in right ascension, and below is a similar plot, made by summing the emission in declination. Positions are measured relative to the nucleus of IC 694, and velocities are measured relative to 3100 km s^{-1}.

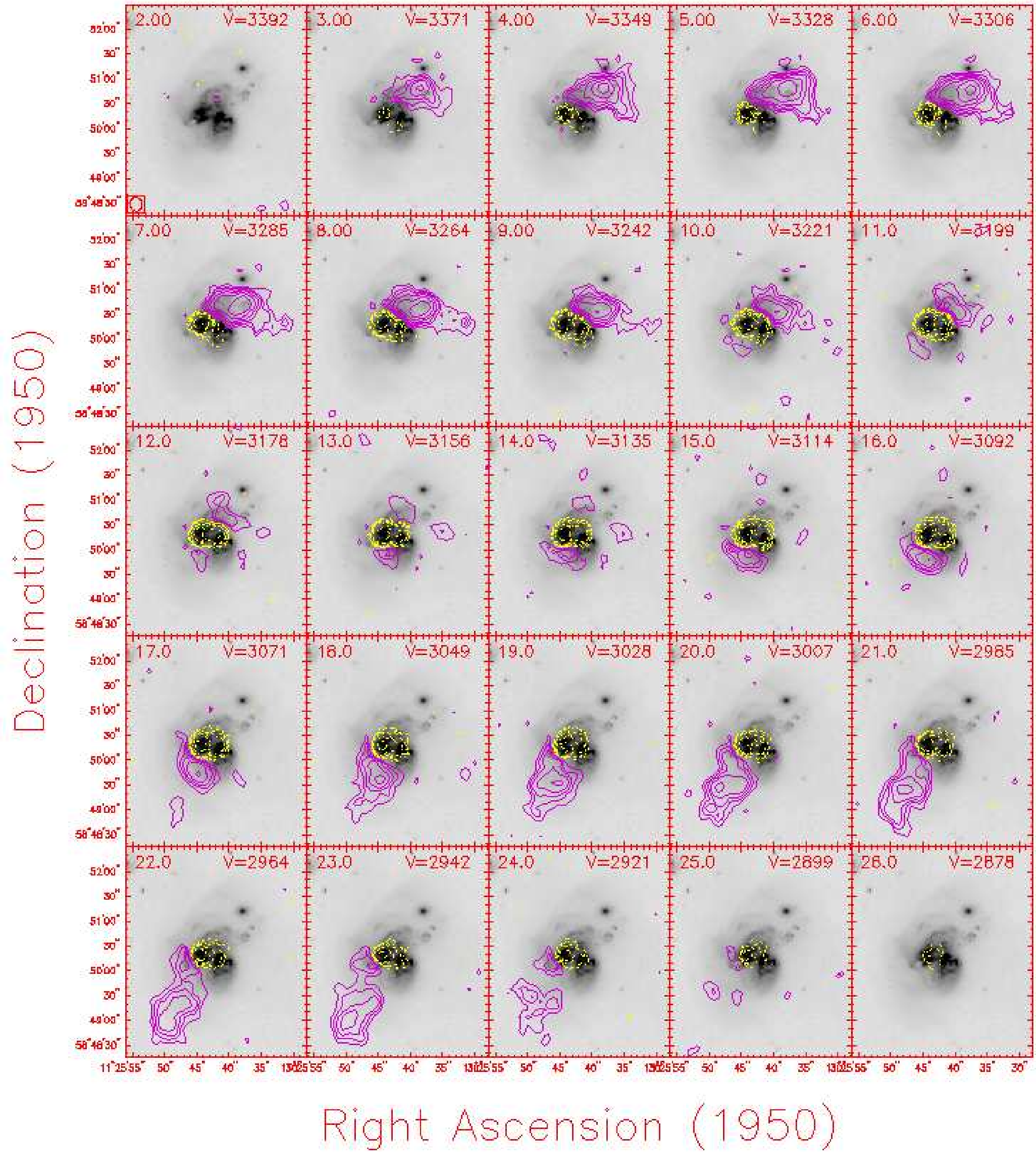

FIG. 3.— H I channel maps of the inner regions of Arp 299 contoured upon the *B*-band image. The higher resolution data are used after Hanning smoothing in velocity by a factor of two to a channel spacing of 21.4 km s^{-1}. The beam size ($17'' \times 15''$) is indicated in the lower left hand corner of the first panel, and each panel is labelled with the channel number and heliocentric velocity. Dotted white lines indicate negative contours, which are drawn at $1\sigma \times$ [-3, -5, -7, -10], where 1σ=0.25 mJy beam^{-1} is the single channel noise level. Positive contours are drawn at $1\sigma \times$ [3, 5, 7, 10], with higher contours drawn a factor of 1.5 times the previous level. The lowest contour corresponds to a column density of 7.2×10^{19}cm^{-2}.

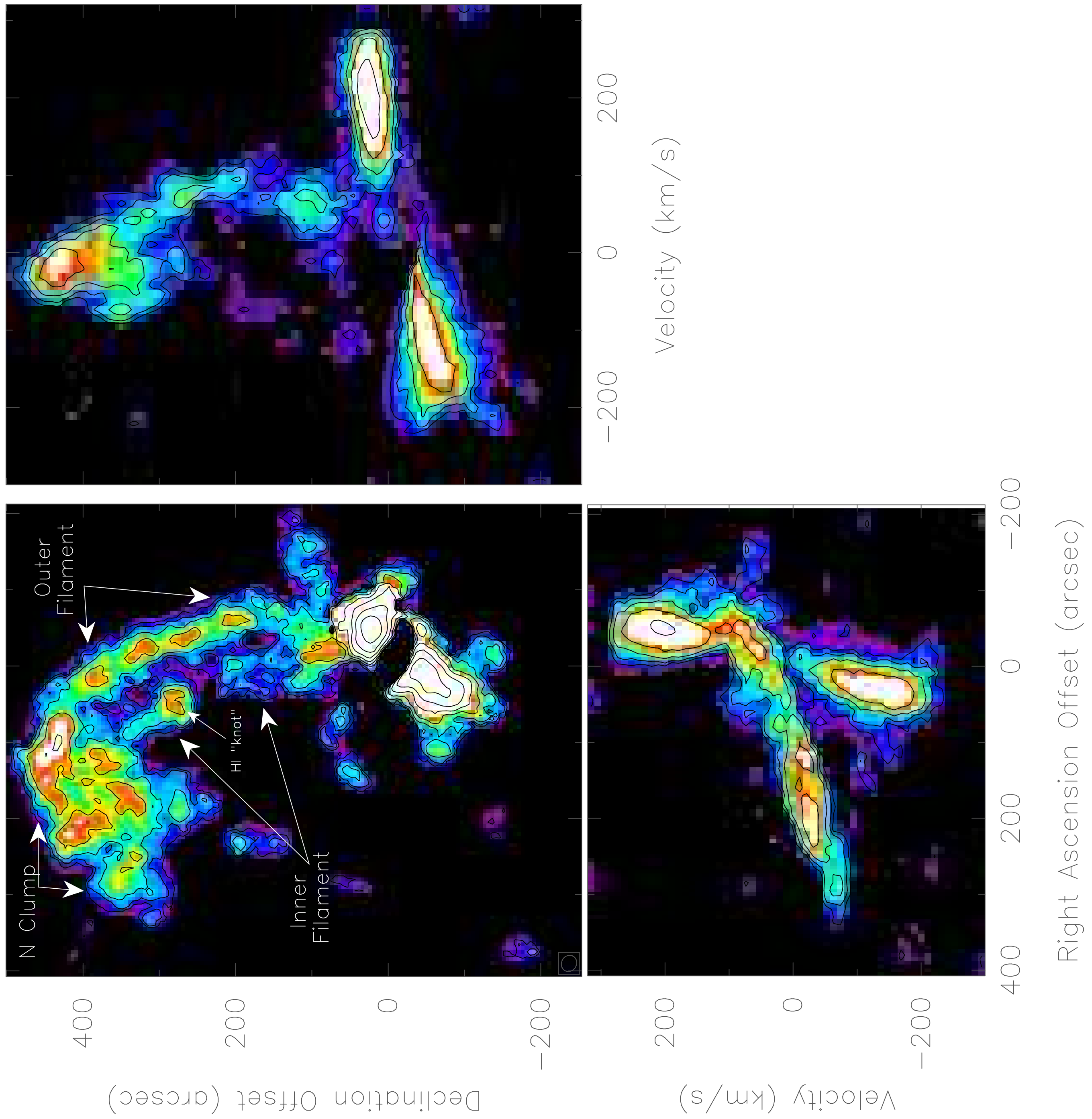

FIG. 4.— Position-Velocity profiles of the entire Arp 299 system, demonstrating the kinematics of the tidal H I features. The top left panel presents a false color and contoured image of the intermediate resolution data cube ($22'' \times 20''$). Features referred to in the text are labelled. The adjacent panels are position-velocity profiles, constructed by summing the data cube in right ascension (right) or declination (bottom). Values below 1σ were not not used when constructing the position-velocity plots. Contours are drawn starting at a level of 8 mJy beam^{-1} km s^{-1} (2×10^{19}cm^{-2}), with higher contours drawn a factor of 2 times the previous level.

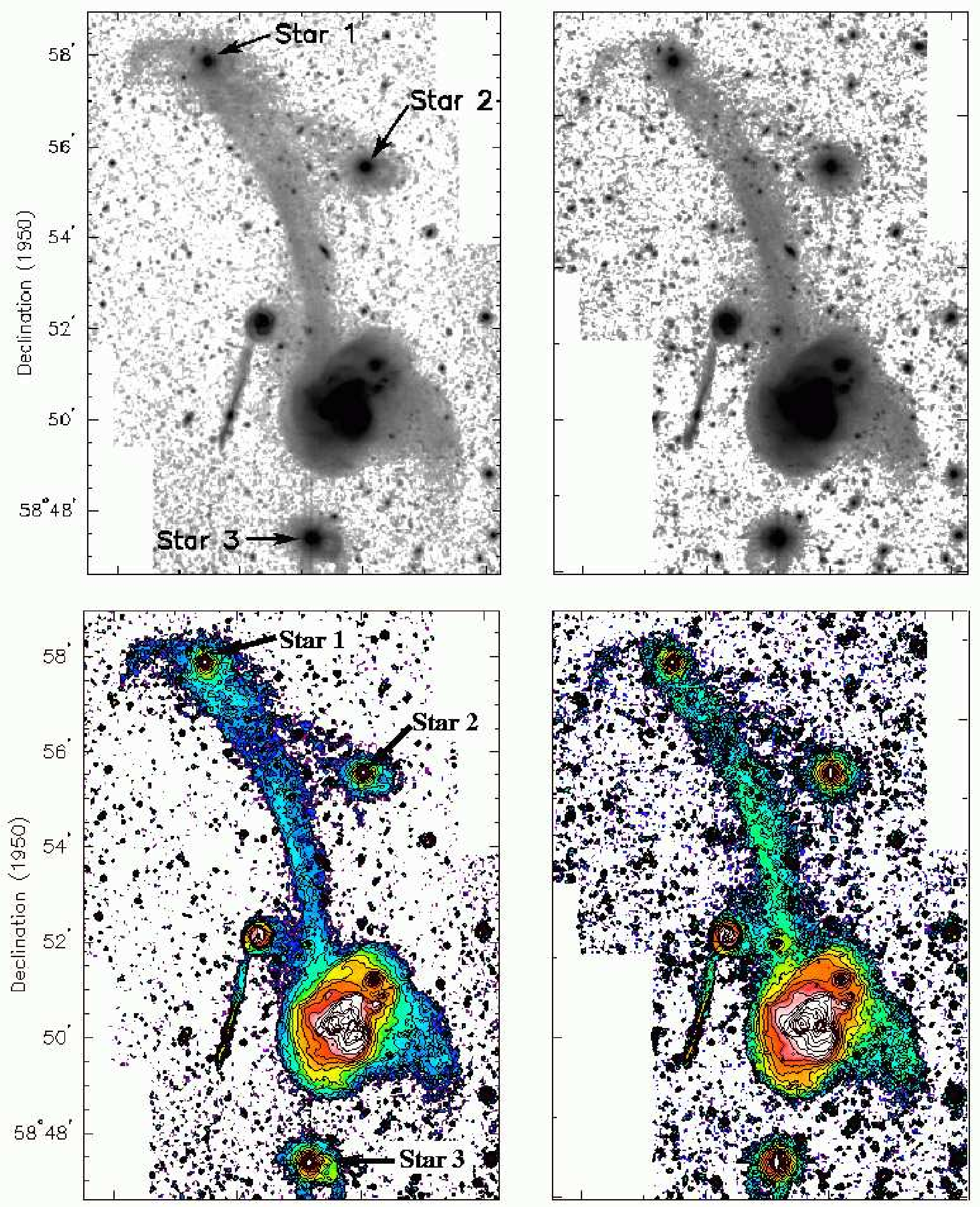

FIG. 5.— Deep optical image of the entire Arp 299 CCD mosaic, showing the total extent of the stellar tail. The deep B- and R-band data are shown on the left and right, respectively, using a logarithmic transfer function. The upper panels (**a & b**) show a greyscaled representation of the data, while the lower panels add contours. The greyscales give a better feeling for the structure at the lowest light levels, while the contoured images provide a quantitative measure of the light peaks. The greyscales cover the range μ_B=28.5 mag arcsec^{-2}– 22.75 mag arcsec^{-2} and μ_R=28.5 mag arcsec^{-2}– 22.0 mag arcsec^{-2}. In panels (c) & (d) black contours are drawn every 1 mag arcsec^{-2} starting at at μ_B=28 mag arcsec^{-2} and μ_R=27 mag arcsec^{-2} and white contours are added every 1 mag arcsec^{-2} starting μ_B=24 mag arcsec^{-2} and μ_R=25 mag arcsec^{-2}. Three stars referred to in the text are labelled in panel (a).

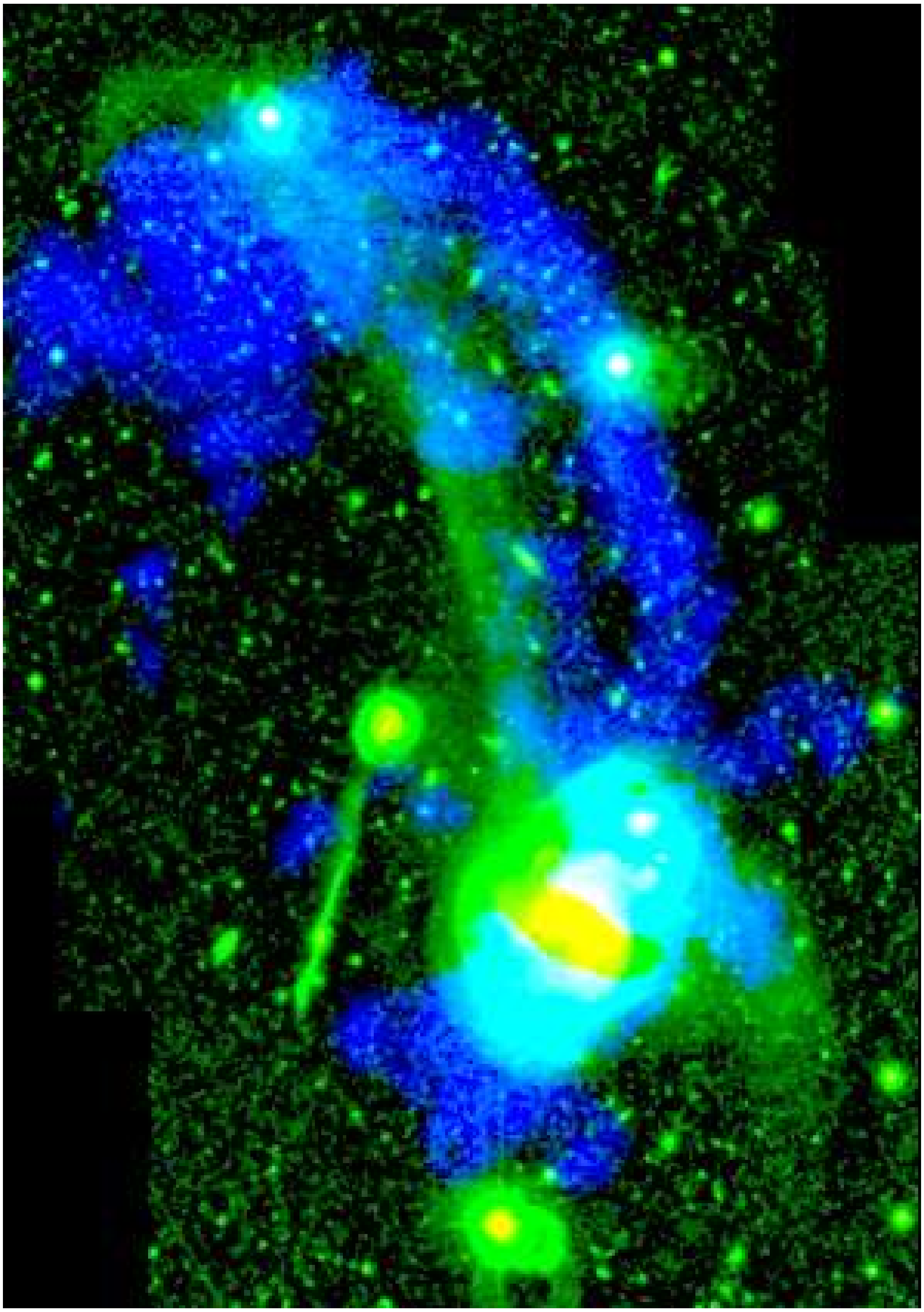

Fig. 6.— An RGB representation of the Arp 299 optical and HI data. Yellow and green indicates optical emission, while blue indicates H I emission. Regions containing both forms of emission appear as the sum of these colors. This figure emphasizes the differences between the stellar and gaseous tidal morphologies.

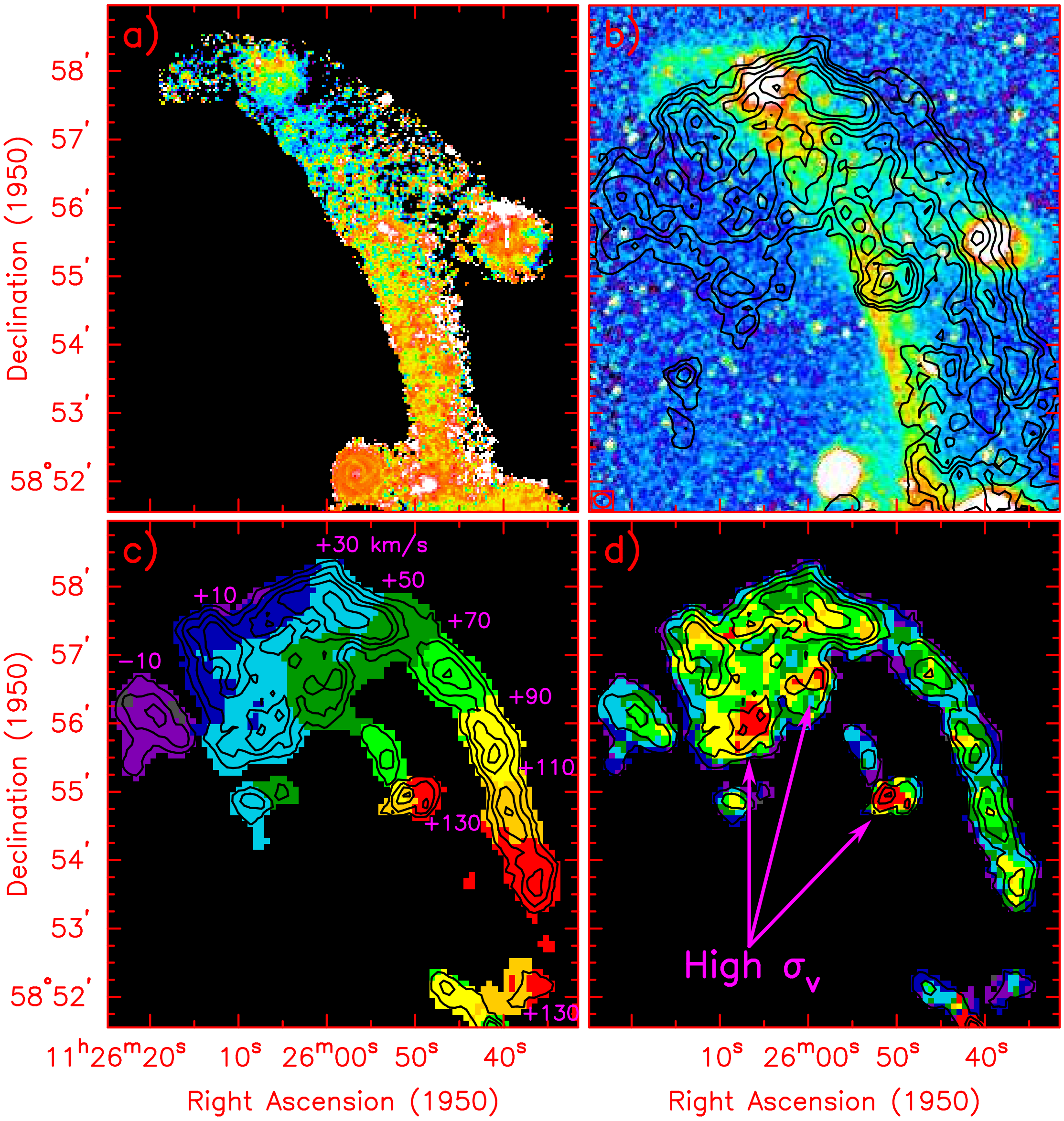

FIG. 7.— Detail of the Arp 299 tidal tail, showing the relationship between the gaseous and stellar morphologies and kinematics. **(a)** B-R color map constructed from the smoothed data using only pixels with a signal to noise greater than or equal to 3 in both the B- and R-band images. A spectral transfer function is used with the following color mappings: Purple: $B-R$ <-0.2 mag, blues: $B-R$ = -0.2 – +1.0; green-yellow: $B-R$ = 1.0 – 2.0 mag; red: $B-R$ >2.0 mag. **(b)** False color rendition of the B-band data with contours of the intermediate resolution data overlaid. Contours are drawn at levels of 4 mJy km s^{-1} beam^{-1} (1×10^{19}cm^{-2}) $\times$[3, 6 10, 15, 20, 25]. **(c)** intensity weighted mean H I line-of-sight velocity. The intermediate resolution data has again been used, but with a higher threshold for the moment algorithm. The color boundaries are indicated with labels giving the velocity (in km s^{-1}) with respect to NGC 3690 ($V_{hel}\approx$3040 km s^{-1}, §3.4). Contours are drawn at (1×10^{20}cm^{-2}) $\times$[1, 1.5, 2, 2.5, 3]. **(d)** H I line-of-sight velocity dispersion, using the same data and threshold as in (c). The colors correspond to the following velocity dispersion ranges: purple–blue = 5–8 km s^{-1}; green = 8–10 km s^{-1}; yellow–orange = 10–13 km s^{-1}; red = 13–20 km s^{-1}. The regions of high velocity dispersion discussed in §3.3 and §4.5 are indicated.

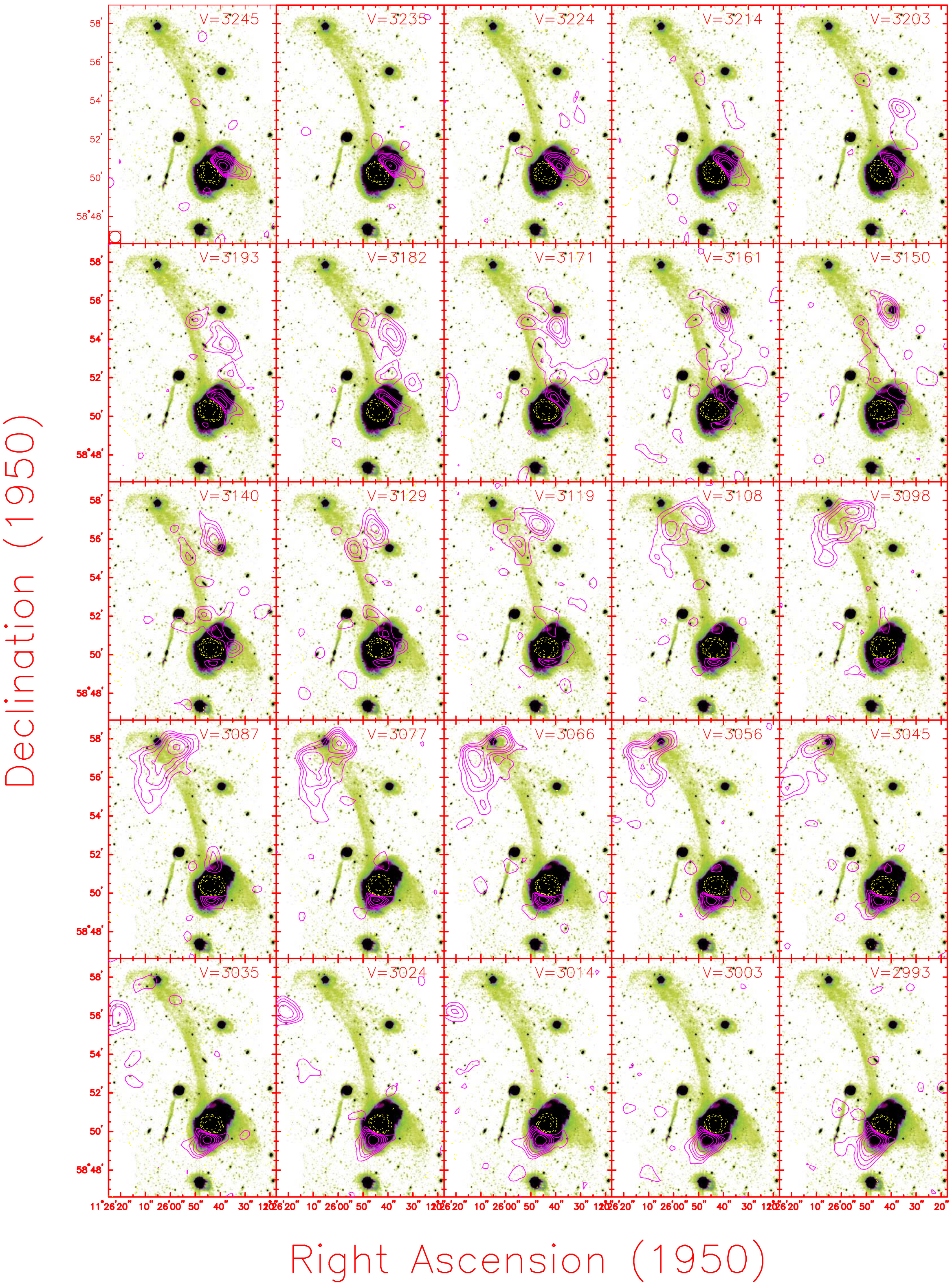

FIG. 8.— Channel maps of the tidal regions of Arp 299 contoured upon the *B*-band image. The greyscales are drawn from μ_B=28.5 mag arcsec^{-2} (white) to 25 mag arcsec^{-2} (black). The more sensitive low-resolution H I cube is used at full velocity resolution (10.52 km s^{-1} channel width). The 35$''$ beam size is indicated in the lower left hand corner of the first panel, and each panel is labelled with the channel number and heliocentric velocity. Dotted yellow lines indicate negative contours, which are drawn at 1$\sigma\times$ [-3, -5, -7, -10], where 1σ=0.37 mJy beam^{-1} is the single channel noise level. Positive contours are drawn at levels of 1$\sigma\times$ [3, 5, 7, 10, 15, 22.5]. The lowest contour corresponds to a column density of 1$\times$10^{19}cm^{-2}. Only channels showing H I emission from the tail are shown.

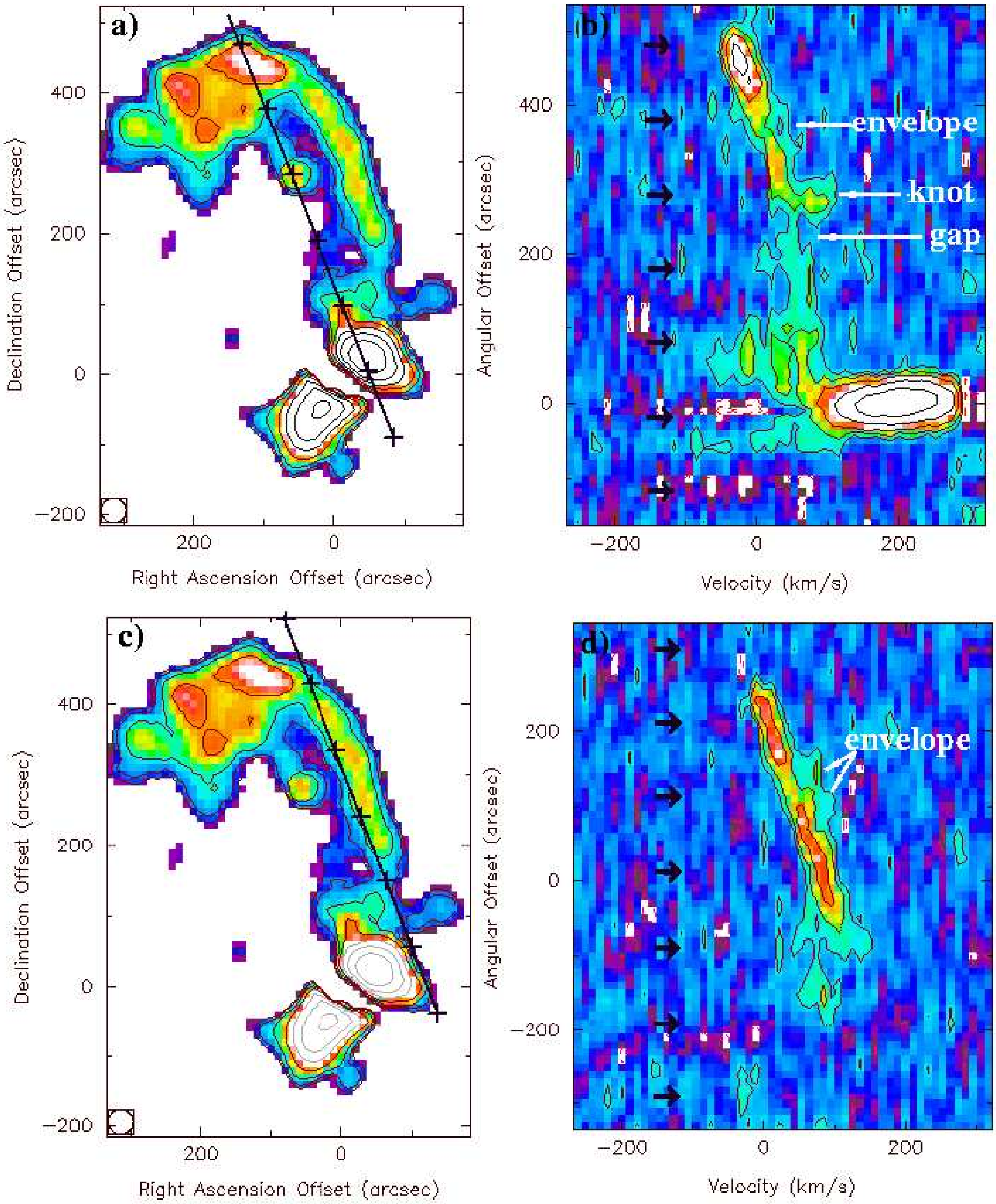

FIG. 9.— Position-Velocity slices taken along both gaseous filaments. The left panels show the location of the slice on the low-resolution H I iintegrated intensity maps, while the right panels show the corresponding position-velocity profile. For the latter, distance along the slice is plotted along the $y-$axis, and velocity with respect to 3100 km s^{-1} is plotted along the $x-$axis. Crosses are drawn at intervals of $100''$ along the slice in the left panel, and arrows indicate the corresponding locations in the right panel. Specific regions referred to in the text are labelled. **(a) & (b)** Position-Velocity slice taken along the inner tidal filament. **(c) & (d)** a similar slice taken along the outer tidal filament.

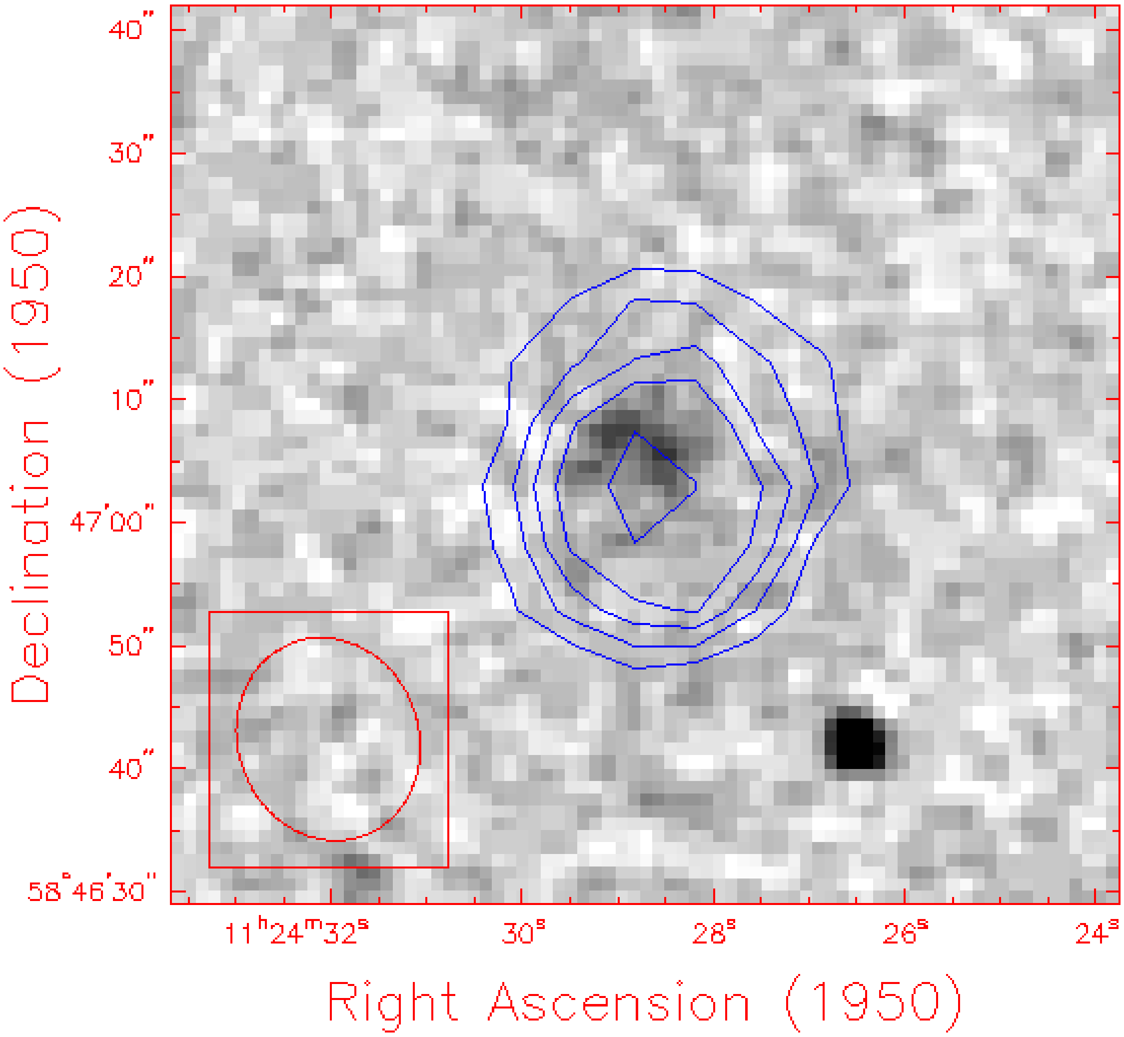

Fig. 10.— Greyscale image of the companion to Arp 299, taken from Version II of the Digitized Sky Survey, with H I contours superimposed. The higher resolution data is used with the $17'' \times 15''$ beam indicated by the ensquared ellipse to the lower left. H I column density contours are drawn at [5, 10, 15, 20, 30] $\times 10^{19}$cm^{-2}.

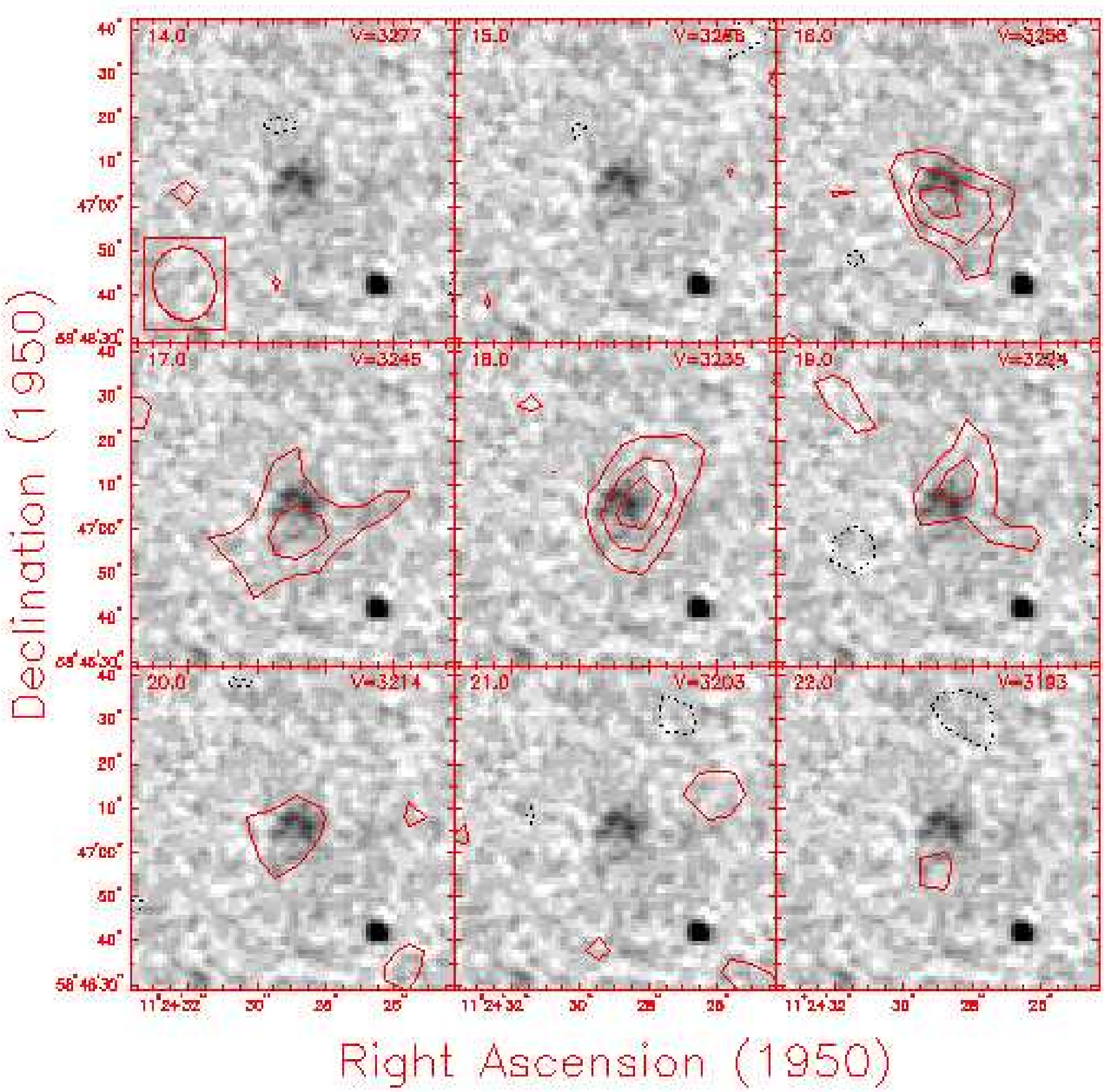

FIG. 11.— H I channel maps of the companion to Arp 299 contoured upon a greyscale of Version II of the Digitized Sky Survey. The higher resolution ($17'' \times 15''$), full velocity resolution (Δv=10.52 km s^{-1}) H I data are used, with the spatial resolution indicated by the ensquared ellipse to the lower left of the first panel. Contours are drawn at 1σ $\times$[-3, 3, 5, 7], where 1σ=0.20 mJy beam^{-1} is the single channel noise level, corresponding to a column density of 9.2×10^{18}cm^{-2}.

TABLE 1
VLA OBSERVING PARAMETERS

Parameter			
Phase Center (α_{1950} δ_{1950})	11^h25^m 44.s2	+58°50′18″	
Velocity Center (Heliocentric)		3080 km s^{-1}	
Primary Beam (FWHM)		30′	
Phase Calibrator		1203+645	
Flux Calibrator		3C268	
Bandwidth		3.125 MHz	
Number of Channels		63	
Channel Separation		10.5 km s^{-1}	
Array Configuration	D	C	C+D
Date	4/18/95	12/10/94	—
Synthesized Beam			
— FWHM: Major Axis × Minor Axis	56″×46″	17″×15″	22″×20″
— Position Angle (East of North)	+37°	−22°	−12°
Time on Source (hrs)	2.1	2.9	5.0
Noise Level (1σ)			
— Flux Density (mJy beam^{-1})	0.56	0.37	0.30
— Column Density ($\times 10^{19}$cm^{-2} beam^{-1} ch^{-1})	0.25	1.7	0.80
— Brightness Temperature (K beam^{-1})	0.13	0.88	0.41

TABLE 2
OPTICAL OBSERVING PARAMETERS

Parameter		
Telescope		UH 88″
Detector		Tek 2048
Readout Mode		binned 1×1
Focal Ratio		f/10
Pixel Size		0.″22
Field of View:		
— Single CCD frame		7.′5 × 7.′5
— Final Image		8.′7 × 12.′4
Date	6/03/95	01/07/96
Filters	*R*	*B*
Effective Exposure Time	$\sim 2 \times 600$ s	$\sim 2 \times 900$ s
Seeing	1.″2	0.″9
Sky Brightness (mag arcsec^{-2})	20.9	22.9
1σ Sky Noise[a] (mag arcsec^{-2})	25.8	27.0
3σ Sky Noise[b] (mag arcsec^{-2})	26.9	28.0

[a] 1σ noise in original unbinned image

[b] 3σ noise after binning 9×9; this should be close to the 3σ detection limit, and we can often trace extended features to 0.5 mag fainter than this.

Table 3
Measured Properties of the Arp 299 System

Quantity	Units	Total	Disk[a]	Tail	Companion[b]
Optical:					
L_B[c]	$(L_{\odot,B})$	4.5×10^{10}	4.3×10^{10}	1.6×10^9	2×10^9
L_R[c]	$(L_{\odot,R})$	4.9×10^{10}	4.7×10^{10}	1.2×10^9	2×10^9
B	(mag)	12.31			18
R	(mag)	11.04			17
H I, measured:					
Velocity Range[d]	(km s^{-1})	2800—3380	2910—3350	3020—3210	3230—3250
$\int Sdv$	(Jy km s^{-1})	17.7	11.7	6.1	0.14
M_{HI}[e]	$(M_\odot)$	9.6×10^9	6.3×10^9	3.3×10^9	8×10^7
M_{HI}/L_B	$(M_\odot\, L_\odot^{-1})$	0.2	0.15	1.6	0.04
M_{HI}/L_R	$(M_\odot\, L_\odot^{-1})$	0.2	0.13	1.7	0.04
H I, corrected[f]					
$\int Sdv$	(Jy km s^{-1})	21.7	15.7		
M_{HI}	$(M_\odot)$	1.18×10^{10}	8.5×10^9		
M_{HI}/L_B	$(M_\odot\, L_\odot^{-1})$	0.3	0.20		
M_{HI}/L_R	$(M_\odot\, L_\odot^{-1})$	0.3	0.18		

[a]Disk values include contribution from minor axis clump and western plume

[b]HI detected companion located at $\alpha_{1950} = 11^h 24^m 28\overset{s}{.}0$, $\delta_{1950} = +58^\circ 48' 05''$ and $v_{\rm hel} = 3245$ km s^{-1}.

[c]Luminosities calculated assuming $M_{\odot,B}$=+5.48 and $M_{\odot,R}$=+4.31. Values for disk are measured to μ_B=26mag arcsec^{-2}, μ_R=25.5mag arcsec^{-2}. Values for tail are measured after removing point sources. The values for the companion are estimated from the DSS image and are very approximate; see text.

[d]Range of H I velocities (heliocentric). Taken from the first-moment image except for the total, which is the range seen in absorption. The uncertainty is ± 5 km s^{-1}.

[e]Integrated H I mass, calculated using $M_{HI} = 2.356 \times 10^5 M_\odot\, \Delta^2 \int Sdv$, where Δ is the distance in Mpc, and $\int Sdv$ is the integrated H I emissivity, in Jy km s^{-1}. Following Sanders, Scoville & Soifer (1991), we adopt 48 Mpc as the distance to Arp 299.

[f]Absorption corrected value; see text.

TABLE 4
GLOBAL QUANTITIES

Quantity	Units	Total	IC 694	NGC 3690
L_B	$L_{\odot,B}$	4.5×10^{10}	2.8×10^{10}	1.7×10^{10}
M_{HI}	$M_{\odot}$	1.18×10^{10}	6×10^{9}	6×10^{9}
M_{H_2}[a]	$M_{\odot}$	1.7×10^{10}	1.1×10^{10}	6×10^{9}
M_{gas}[b]	$M_{\odot}$	3.9×10^{10}	2.3×10^{10}	1.6×10^{10}
M_{HI}/L_B	$M_{\odot}\, L_{\odot,B}^{-1}$	0.3	0.2	0.4
M_{H_2}/L_B	$M_{\odot}\, L_{\odot,B}^{-1}$	0.4	0.4	0.4
M_{gas}/L_B	$M_{\odot}\, L_{\odot,B}^{-1}$	0.9	0.8	0.9
M_{H_2}/M_{HI}		1.4	1.8	1.0
L_{IR}[c]	$(L_{\odot,bol})$	7.9×10^{11}		
L_{IR}/L_B		18		
L_{IR}/M_{H_2}	$(L_{\odot}\, M_{\odot}^{-1})$	69		

[a]From Casoli et al. (1999), converting to our distance and a CO-to-H_2 conversion factor of $3 \times 10^{20}\,\mathrm{cm}^{-2}\,(\mathrm{K\,km\,s}^{-1})^{-1}$. We have equally divided the gas located at the overlap region $C - C'$ between IC 694 and NGC 3690, and assigned the "widespread" emission to IC 694.

[b]Total gas mass corrected for the presence of He: $M_{gas} = 1.36 \times (M_{H_2} + M_{HI})$

[c]Far infrared luminosity over the range 8—1000μm, from Sanders et al. (1991).